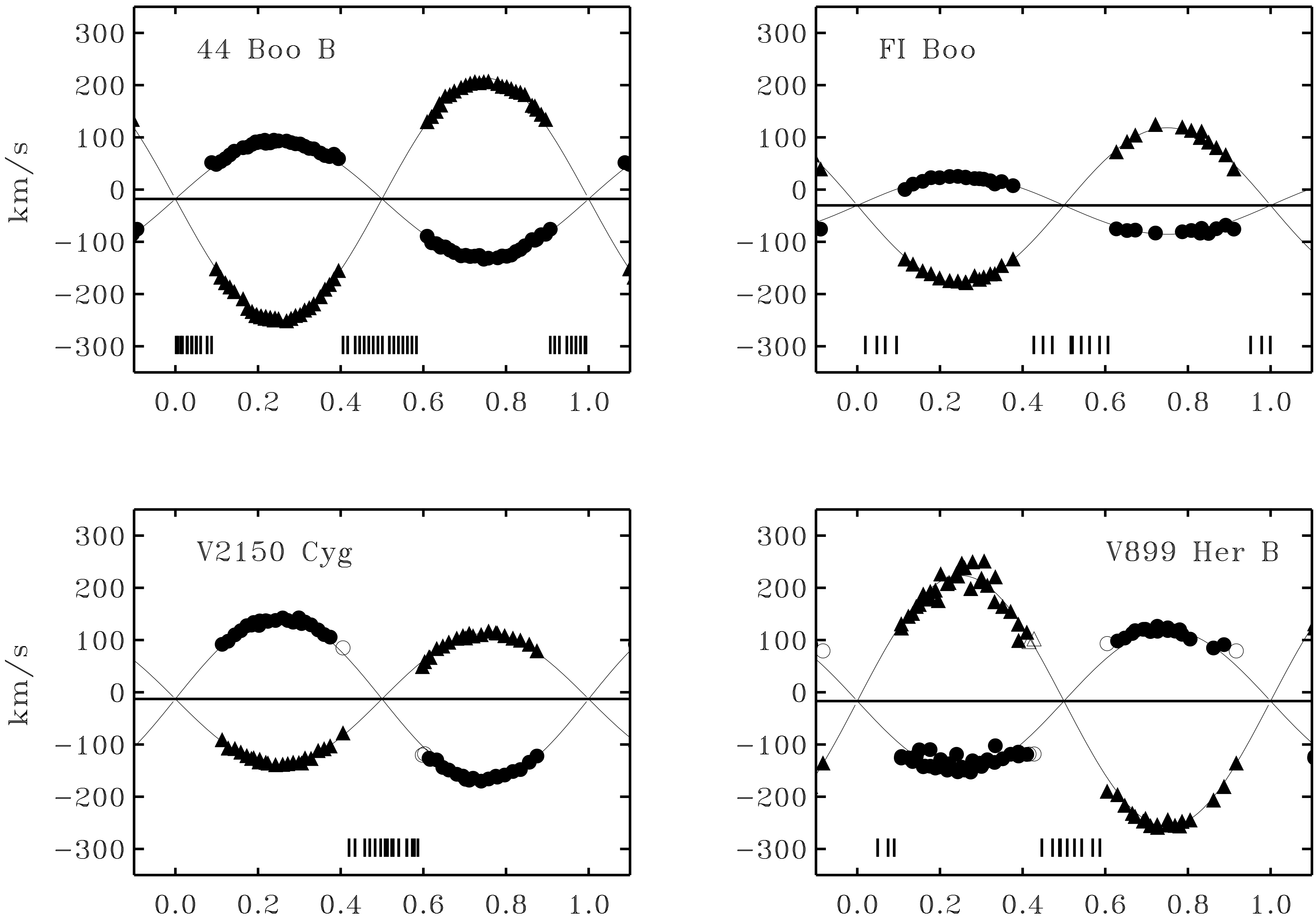

44 Boo B
FI Boo
V2150 Cyg
V899 Her B
km/s
300
200
100
0
−100
−200
−300
0.0
0.2
0.4
0.6
0.8
1.0

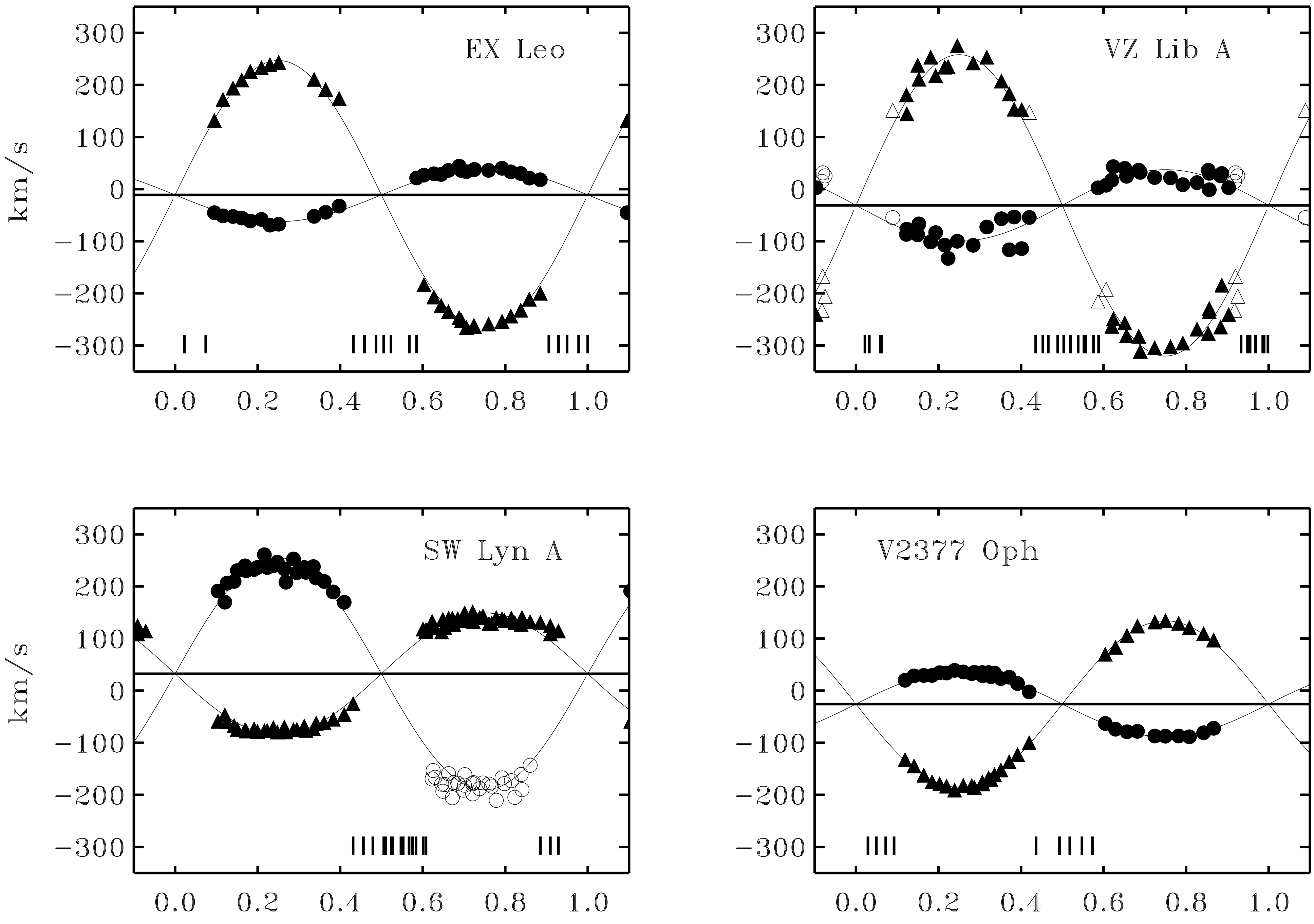
EX Leo
VZ Lib A
SW Lyn A
V2377 Oph
km/s
km/s

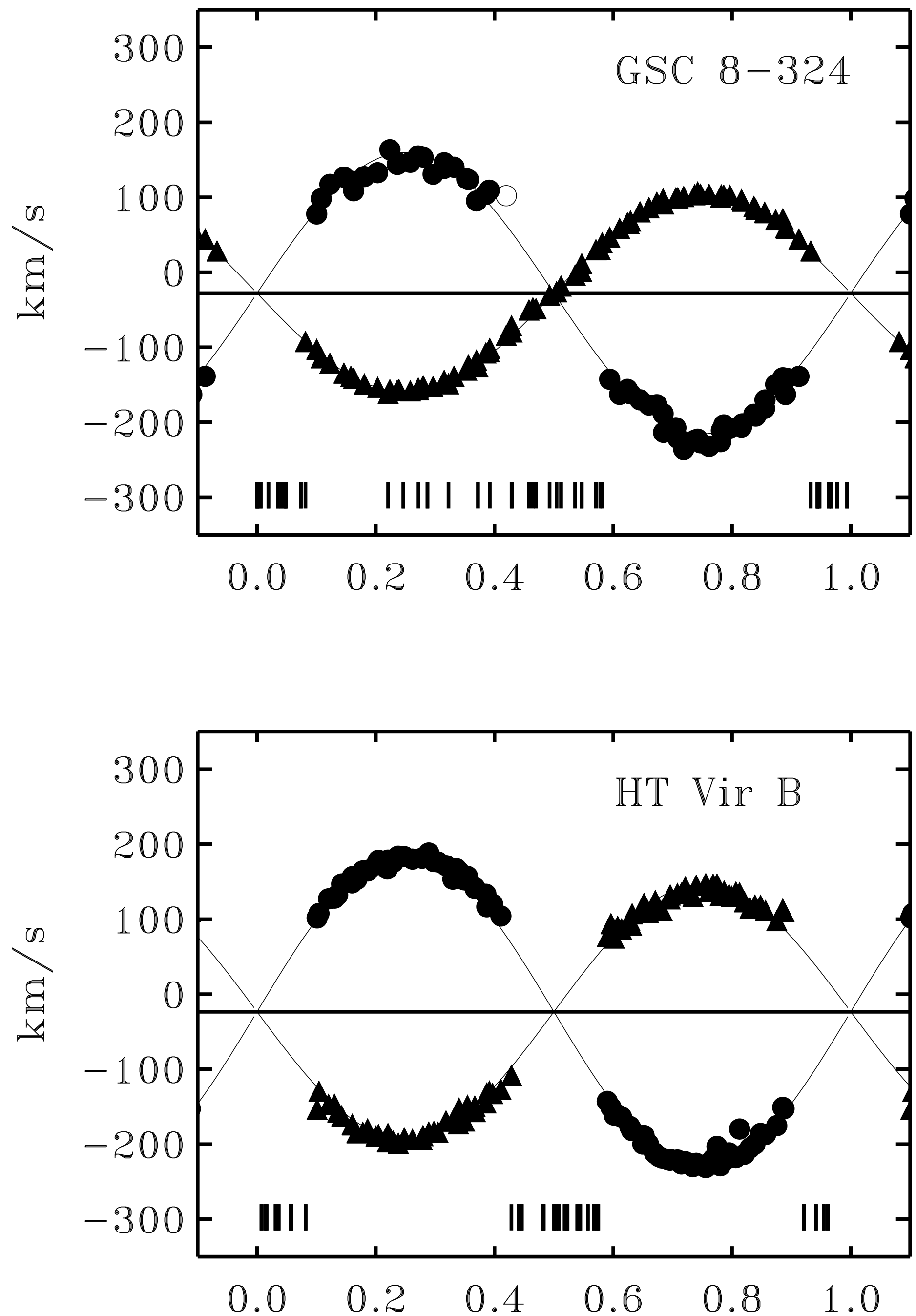
GSC 8−324
HT Vir B
km/s
300
200
100
0
−100
−200
−300
0.0
0.2
0.4
0.6
0.8
1.0

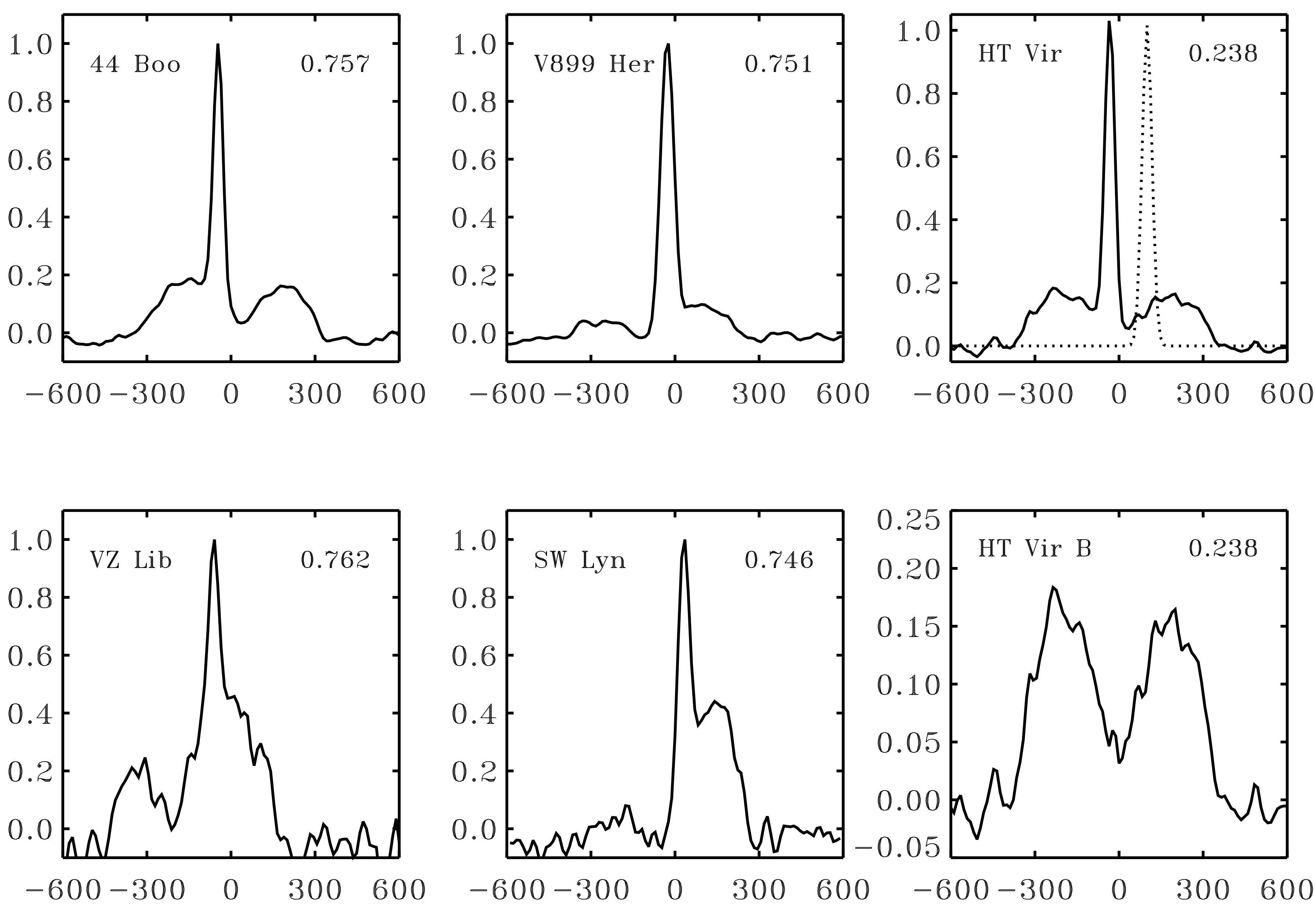
44 Boo
0.757
V899 Her
0.751
HT Vir
0.238
VZ Lib
0.762
SW Lyn
0.746
HT Vir B
0.238
−600 −300 0 300 600

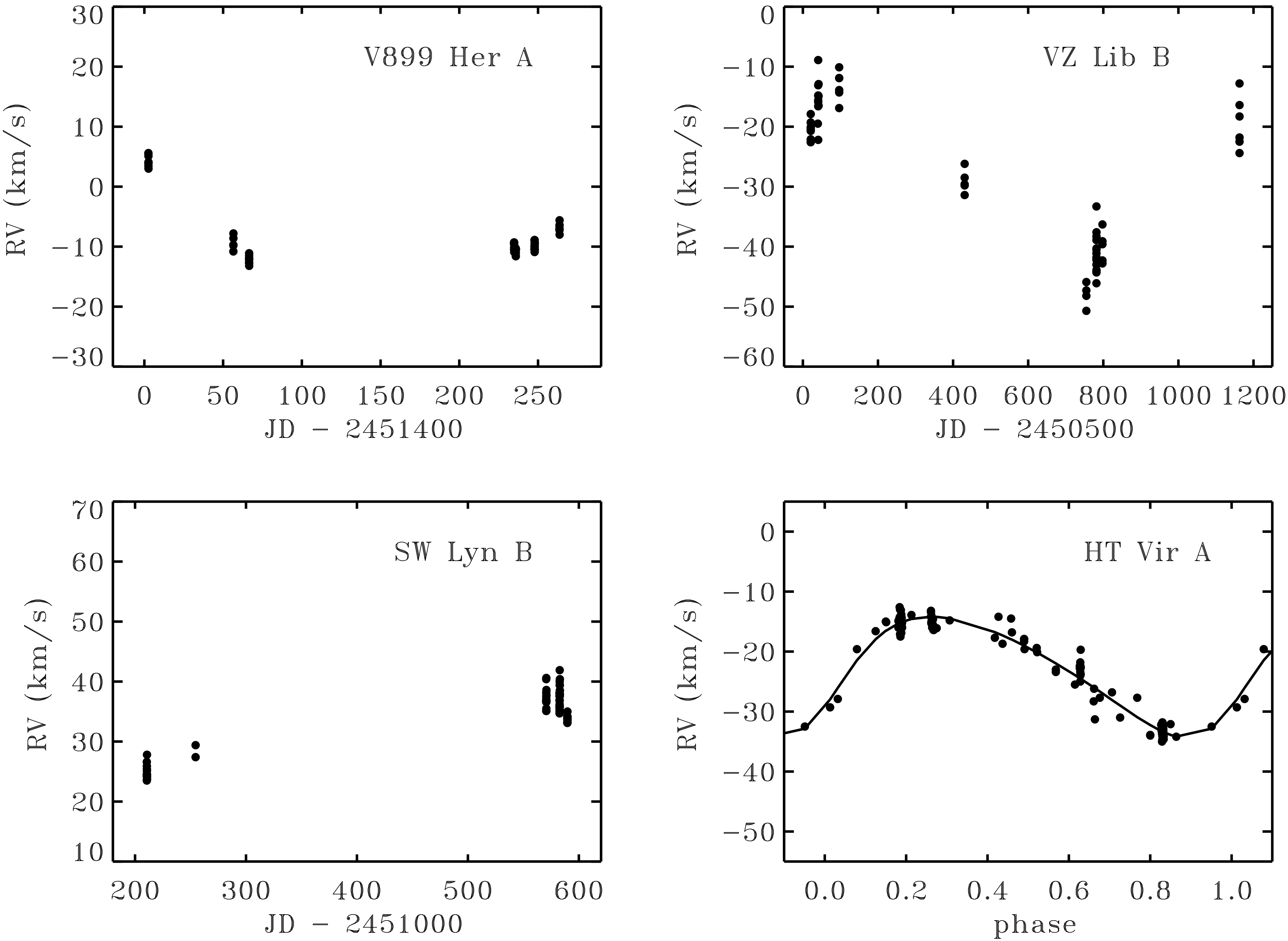
V899 Her A
RV (km/s)
JD − 2451400
VZ Lib B
RV (km/s)
JD − 2450500
SW Lyn B
RV (km/s)
JD − 2451000
HT Vir A
RV (km/s)
phase

Radial Velocity Studies of Close Binary Stars. IV[1]

Wenxian Lu[2] and Slavek M. Rucinski

David Dunlap Observatory, University of Toronto
P.O.Box 360, Richmond Hill, Ontario, Canada L4C 4Y6

`lu,rucinski@astro.utoronto.ca`

and

Waldemar Ogłoza

Mt. Suhora Observatory of the Pedagogical University
ul. Podchorażych 2, 30-084 Cracow, Poland
and N.Copernicus Astronomical Center
ul. Bartycka 18, 00-716 Warszawa, Poland

`ogloza@wsp.krakow.pl`

ABSTRACT

Radial-velocity measurements and sine-curve fits to the orbital velocity variations are presented for the fourth set of ten close binary systems: 44 Boo, FI Boo, V2150 Cyg, V899 Her, EX Leo, VZ Lib, SW Lyn, V2377 Oph, Anon Psc (GSC 8-324), HT Vir. All systems are double-lined spectroscopic binaries with only two of them not being contact systems (SW Lyn and GSC 8-324) and with five (FI Boo, V2150 Cyg, V899 Her, EX Leo, V2377 Oph) being the recent photometric discoveries of the Hipparcos satellite project. Five of the binaries are triple-lined systems (44 Boo, V899 Her, VZ Lib, SW Lyn, HT Vir). Three (or possibly four) companions in the triple-lined systems show radial-velocity changes during the span of our observations suggesting that these are in fact quadruple systems. Several of the studied systems are prime candidates for combined light and radial-velocity synthesis solutions.

Subject headings: stars: close binaries - stars: eclipsing binaries – stars: variable stars

---

[1]Based on the data obtained at the David Dunlap Observatory, University of Toronto.

[2]Current address: NASA/GSFC, Mailstop 664, 8800 Greenbelt Road, Greenbelt, MD 20771

1. INTRODUCTION

This paper is a continuation of the radial-velocity studies of close binary stars, Lu & Rucinski (1999, Paper I), Rucinski & Lu (1999, Paper II) and Rucinski et al. (2000, Paper III). The main goals and motivations are described in these papers. In short, we attempt to obtain radial-velocity data for close binary systems which are accessible to 1.8-m class telescopes at medium spectral resolution of about R = 10,000 – 15,000. Selection of the objects is quasi-random in the sense that we have started with short period (mostly contact) binaries and we attempt to slowly progress to longer periods as the project continues. We publish the results in groups of ten systems as soon as reasonable orbital elements are obtained from measurements evenly distributed in orbital phases.

This paper is structured in the same way as Papers I – III in that most of the data for the observed binaries are in two tables with the radial-velocity measurements (Table 1) and their sine-curve solutions (Table 2). Section 2 of the paper contains brief summaries of previous studies for individual systems. The special feature of this paper which distinguishes it from the previous three papers is a discussion of close spectroscopic/visual companions to five close systems in Section 3. We found many similarities in these triple-lined systems and decided to publish them together in one installment of our series. Table 3 lists the radial-velocity data for the companions which we always call the "third components" of the systems. In this spirit, we will discuss their luminosities in relation to those of the close binaries, L_3/L_{12}. We utilize the conventional naming of such components in visual systems with A signifying the brighter component in a close visual pair (HT Vir turns out to be an exception).

The observations reported in this paper have been collected between February 1997 and October 2000; the ranges of dates for individual systems can be found in Table 1. Eight systems discussed in this paper have been observed for radial-velocity variations for the first time. 44 Boo and SW Lyn have been observed before; for both, we are providing much improved radial-velocity orbits.

We derive the radial-velocity data using the *broadening function* (BF) approach of the linear Singular Value Decomposition (SVD), as described in Rucinski (1999)[3]. The two peaks of the BF are fitted by Gaussians giving radial velocities of the components. Then, variations of the radial velocities are represented by sine curves giving the center-of-mass velocity, V_0, the two semi-amplitudes, K_1 and K_2, and the phase of the primary eclipse, T_0. Since our initial goals were the values of V_0 and of the mass-ratio $q = K_1/K_2$, this approach was deemed adequate when we started the program. We are aware that the amplitudes and hence the masses may be biased by the Gaussian approximation, but we are unable to do the full modeling (as was done for AW UMa, AH Vir and W UMa: Rucinski (1992); Lu & Rucinski (1993); Rucinski et al. (1993)), without knowledge of the degree-of-contact and of the orbital inclination which are derivable from light curves. Thus, we continue using the Gaussians recognizing that one day our values of the semi-

[3]Practical advice and detailed suggestions are available also in http://www.astro.utoronto.ca/∼rucinski/.

amplitudes may have to be corrected for systematic inaccuracies of our measurements.

The data in Table 2 are organized in the same manner as before. In addition to the parameters of spectroscopic orbits, the table provides information about the relation between the spectroscopically observed epoch of the primary-eclipse T_0 and the recent photometric determinations in the form of the (O–C) deviations for the number of elapsed periods E. It also contains our new spectral classifications of the program objects (unless taken in parentheses when we use other spectral type estimates).

For further technical details and conventions used in the paper, please refer to Papers I – III of this series.

2. RESULTS FOR INDIVIDUAL SYSTEMS

2.1. 44 Boo B

With the large parallax of $p = 78.4 \pm 1.0$ milli-arcsec (mas) (ESA 1997, HIP), 44 Boo B[4] is the nearest contact binary and one of the nearest close binaries. Because of its brightness, it has been one of the most frequently photometrically observed variable stars in the sky. 44 Boo B is the fainter component of a relatively close (currently 1.7 arcsec) visual double which is attracting vigorous observational activity in the fields of stellar interferometry and speckle-interferometry. We do not relate to these studies because our radial-velocity data have been obtained in a short interval of only 10 days so that they contribute only one radial-velocity data point of the long-period (225 year), visual orbit.

Several studies attempted to determine a radial-velocity orbit for 44 Boo B. These efforts are summarized in Hill et al. (1989). Here we present results far superior to any previous attempts. The success is mostly due to extraction of the component velocities using the broadening function approach (see Section 3) which permitted excellent separation of the three spectral components in the system. In particular, we provide an accurate estimate of the mass ratio for 44 Boo B, $q_{sp} = 0.487 \pm 0.006$, which should be of much help in future photometric studies of the contact system. The radial-velocity orbit is shown graphically in Figure 1.

Since the discovery (Schilt 1926), the presence of the brighter companion created problems in studies of the close pair. The most extensive study of 44 Boo system by Hill et al. (1989) discussed efforts of de-coupling of the spectral and photometric signatures of the visual pair, but even such basic data as spectral types or color indices were difficult to derive. The re-analysis of the Hipparcos data for close visual binaries (Fabricius & Makarov 2000), gave reliable magnitudes and color indices for both components, $V^A = 5.28$, $(B-V)^A = 0.65$ and $V^B = 6.12$, $(B-V)^B = 0.94$; the magnitudes

[4]The star 44 Boo has another name, i Boo. Frequently, these are combined, which is incorrect and makes electronic searches difficult. We use only the former name in this paper.

are the average ones so that they do not take into account the variability of component B. The color index for component A agrees with the estimate of the spectral type by Hill et al. (1989) of G1V while the color index for component B points at a much later spectral type than was considered before, around K2V, in accordance with the well known high magnetic activity of the contact system.

The magnitude difference at maximum of 44 Boo B relative to component A was estimated by Hill et al. (1989) as $\Delta V = 0.63$, so that $V^B(max) = 5.91$. For this brightness, the absolute magnitude predicted from the parallax is $M_V^B = 5.38{\pm}0.04$, whereas the prediction of the $M_V(\log P, B{-}V)$ calibration (Rucinski & Duerbeck 1997, RD97) is $M_V^B(cal) = 5.50$. These estimates would agree at $M_V^B = 5.38$ if we use $(B{-}V) = 0.90$ in the calibration, assuming that the maximum light $(B{-}V)$ is slightly smaller (bluer) than the average value given by Fabricius & Makarov (2000). We note that 44 Boo B, in spite of its proximity, was used in the first $M_V(\log P, B - V)$ with some reservations (Rucinski 1994) because its color index was poorly know at that time. It is gratifying to see now a much better agreement of the directly determined M_V for 44 Boo B with the calibration.

2.2. FI Boo

FI Boo is a new discovery from the Hipparcos satellite mission. Duerbeck (1997) included it in the list of possible contact binaries. The period reported in the Hipparcos Catalogue is equal to one half of the orbital period that we find and the zero epoch T_0 was given in the Catalogue for the maximum light. With our spectroscopic results, the contact system is of the W-type, with the less massive component eclipsed at the eclipse given by T_0, which has been selected to be one quarter of the orbit before the maximum given in HIP.

The radial-velocity orbit for FI Boo is very well determined (Figure 1). The small value of $(M_1 + M_2)\sin^3 i = 0.343 \pm 0.010\,M_\odot$ is consistent with the small photometric amplitude of about 0.15 mag. in suggesting a low orbital inclination.

Assuming $V_{max} = 9.57$ on the basis of the average V in Hog (2000, TYC2) and the amplitude in HIP, with the parallax of $p = 9.52{\pm}2.10$ mas, we obtain $M_V = 4.41{\pm}0.49$. The RD97 calibration gives $M_V(cal) = 4.17$.

2.3. V2150 Cyg

V2150 Cyg has been discovered by the Hipparcos satellite mission. It shows a small photometric amplitude of 0.12 mag. suggesting a low orbital inclination. This is in accord with the low value of $(M_1 + M_2)\sin^3 i = 1.376 \pm 0.018\,M_\odot$ for an early spectral type of the binary which suggests a rather massive system. Abt (1981) estimated the spectral type to be A5V; our independent estimate is A6V. The orbital period is 0.591 days and the HIP light curve looks like of a genuine contact binary,

which is a rare occurrence among such early-type systems.

Although the system is a visual double (ADS 14835), its orientation relative to the spectrograph slit was such that we were able to avoid the faint ($\Delta m = 3.4$) companion at the separation of 3.7 arcsec.

Our radial-velocity orbit is very well determined (Figure 1). The contact system consists of two very similar components with $q = 0.802 \pm 0.006$ with a more massive component eclipsed at the primary minimum (type A). The only previous radial-velocity measurements of V2150 Cyg, in a survey by Grenier et al. (1999), showed scatter among three measurements indicating radial-velocity variability: $V = 31.4 \pm 16.8$ km s^{-1}. The nominal accuracy of this survey was 3.0 km s^{-1} on the basis of spectra with resolution about 8 times lower than ours.

In spite of a good solution of the radial-velocity orbit, we found one disturbing feature of the solution for V2150 Cyg: The radial-velocity amplitudes depend on the spectral type of the template star used to derive the broadening functions. This is unusual because for most W UMa-type systems we have not seen any dependence of the amplitudes on the spectral type. Normally, with some spectral-type mismatch of the template, the broadening function could change its intensity scale and its quality of determination, but the radial-velocity amplitudes would stay constant. We selected several sharp-line standards from the list of Dr. Frank Fekel (private communication). Over the range of the template spectral types within the A-type, we see a change of up to 7% in both semi-amplitudes K_i, with larger amplitudes obtained with templates of earlier spectral types. While the mass-ratio remained perfectly constant, the systematic uncertainty in the amplitudes would obviously affect the derived values of masses. We have no explanation of the effect, but note that V2150 Cyg is of the earliest spectral type among binary systems analyzed by us so far.

The system of V2150 Cyg is important because it may provide an crucial extension of the absolute magnitude calibration $M_V(\log P, B-V)$ toward early spectral types. With $V_{max} = 8.06$ estimated from the average data in TYC2 and the amplitude, and with the parallax $p = 4.7 \pm 1.6$ mas, we obtain $M_V = 1.43 \pm 0.74$ while the RD97 calibration, pushed to a color index as blue as $(B-V) = 0.25$, gives $M_V(cal) = 1.89$. A big question is obviously the amount of reddening for this relatively distant (about 210 pc) system. The color index, when compared with the spectral type A5/6 V, suggests a moderate reddening of about $E_{B-V} = 0.07$. In this case, the absolute magnitude derived from the parallax is $M_V = 1.21 \pm 0.74$, while $M_V(cal) = 1.67$.

2.4. V899 Her B

V899 Her is the next Hipparcos discovery. Although it is classified in the Hipparcos catalogue as an EB light-curve system (with unequal minima), it seems to be a genuine contact binary with a low-amplitude (0.14 mag.) EW light curve and practically equally deep eclipses. Apparently, the light curve classification was driven by one deviating point, possibly a photometric error. We have kept the Hipparcos ephemeris which leads to an A-type contact system.

We discovered that V899 Her is a spectroscopically triple system in which the contact binary is the fainter component, so that we designate the contact system as component B. The broadening function was an indispensable tool in separating the three spectral components; without it, the system would be probably unsolvable (see Section 3). The presence of the bright companion explains the inconsistency between large radial-velocity amplitudes of the components of V899 Her B, leading to a large value of $(M_1+M_2)\sin^3 i = 2.33\pm0.08\,M_\odot$ (and thus an indication of the orbital inclination close to 90°) and the small photometric amplitude of the W UMa-type light curve which appears to be “diluted” in the total systemic light.

The spectral type that we estimated from our low-resolution classification spectra is F5V, with indications of a contribution from the fainter G-type component. Because of the dominance of the third component, there is no point to apply the RD97 calibration to this case. The maximum brightness and the color index, $V_{max} = 7.87$, $(B-V) = 0.48$ almost certainly reflect the properties of the third star rather than that of the close binary.

Because of the presence of the bright companion, the radial-velocity orbit of V899 Her B is not as well defined as for other close binaries (Figure 1). The bright companion A is itself a radial-velocity variable because we noticed well defined variations within the 250 day span of our observations (see Section 3). We do not see these variations in the systemic velocity of the close pair, so we assume that the visual companion is itself an independent spectroscopic binary.

2.5. EX Leo

EX Leo has been found by Hipparcos. Our solution (Figure 2) describes a rather typical contact binary of the A-type with a small mass-ratio, $q = 0.199 \pm 0.036$. Our estimate of the spectral type, F6 V, agrees very well with $(B-V) = 0.53$ from TYC2. The light curve has an amplitude of about 0.25 mag. and is quite well defined, but perhaps a bit sparsely covered by the HIP data.

The parallax $p = 9.84 \pm 1.11$ mas with $V_{max} = 8.17$ leads to $M_V = 3.13 \pm 0.26$ so that it agrees with the RD97 calibration, $M_V(cal) = 3.45$.

2.6. VZ Lib A

VZ Lib has been known as a contact binary since the work of Tsesevich (1954). Claria & Lapasset (1981) published the last currently available photometric study of the system.

We have detected a spectroscopic companion to VZ Lib, about five times fainter than the contact binary. We discuss it in Section 3. Here we note that this component may have a slowly variable radial velocity, but these variations are not reflected in the systemic velocity of the close binary.

It is impossible to derive the correct V_{max} for the contact binary value because of the poorly known contribution of the third component to the total systemic light. The observed combined brightness, $V_{max} = 10.36$, $(B - V) = 0.61$ (Claria & Lapasset 1981) is accord with our estimate of the spectral type, G0 (composite). These data, together with the HIP parallax $p = 4.92 \pm 1.96$ mas imply $M_V = 3.59 \pm 0.88$ for the whole system while the RD97 calibration for the contact system predicts $M_V(cal) = 3.94$ which is in agreement with some contribution of the third star to the systemic brightness.

Because of the faintness of the system, presence of the third component, and difficulties of measuring velocities of the close binary, our radial-velocity solution is relatively poor (Figure 2). The system appears to be a contact binary of the A-type with a moderately small mass-ratio of $q = 0.24 \pm 0.07$. The orbit is probably oriented close to edge-on because the sum of masses is relatively large, $(M_1 + M_2)\sin^3 i = 1.70 \pm 0.12\, M_\odot$.

We note that our spectroscopically derived moment of the primary eclipse deviates by about 2 hours from the ephemeris of Claria & Lapasset (1981), either due to period changes or accumulated errors in the period over the long time since the last photometric observations.

2.7. SW Lyn A

The binary was discovered as a variable star by Hoffmeister (1949). Major photometric studies were done by Vetešnik (1968, 1977). Recently, Ogłoza et al. (1998) re-discussed the extant data; the discussion was to a large extent guided by the spectroscopic results of Vetešnik (1977) in that a mass-ratio was assumed to be around $q \simeq 0.35$, in spite of photometric solutions which tended to converge to $q \simeq 0.5 - 0.6$. In fact, our spectroscopic results do give $q_{sp} = 0.52 \pm 0.03$.

From the spectroscopic point of view, SW Lyn is quite complex: It appears to be a very close, short-period Algol system with a faint, but detectable secondary. We also clearly see a third component, about three times fainter than the close binary, which has not previously been detected spectroscopically (see Section 3). Possibly, it is the same star which is producing the 2128 day periodicity in the eclipse timing (Ogłoza et al. 1998).

Our radial-velocity orbit is entirely different from that of Vetešnik (1977) which was obtained at a very low spectral resolution. Thus, we do not confirm any manifestations of apparent eccentricity which were explained by gas streams. In view of our results, the detailed discussion of the physical properties of the system by Ogłoza et al. (1998) may have to be revised. We did experience difficulties in measuring velocities of the secondary component whose signal in the broadening function is very weak in comparison with the third star and the primary component (see Section 3). These difficulties were especially severe in the second half of the orbit. Thus, in order not to affect the systemic velocity V_0 in our combined orbital solution which takes into account the velocities of both stars, we assigned weights of one-half and one-quarter to all measurements of the secondary within the first and second halves of the orbit, respectively (Figure 2).

Our observations were obtained in two groups (16 and 55 observations) separated by one year which – in view of the presence of the third star – poses a question whether the observations of the close binary could be combined in one solution. Accordingly, we obtained one solution based on all observations and one based only on the 55 observations of the second season (the phase distribution for the first season did not permit a separate solution). The results do not differ significantly, indicating that the center of mass of the close binary probably did not move much between the seasons. However, the conjunction times came out different, but within the combined errors of both solutions. For reference, we give here the results of the solution based only on the second season: $V_0 = +31.11(1.26)$, $K_1 = 116.09(1.52)$, $K_2 = 222.87(3.60)$, $T_0 = 2,451,400.1752(22)$.

The photometric properties of SW Lyn are rather poorly known. Vetešnik (1968) estimated $V_{max} = 9.2$ and $(B-V) = 0.38$. The color index corresponds to the spectral type of F2 V. However, TYC2 suggests the mean $(B-V) = 0.23$. With its period of 0.644 days, SW Lyn is of interest to studies of the short period Algol systems.

Our spectroscopic value of T_0 agrees very well with the recent photometric timing of Ogłoza et al. (2000).

2.8. V2377 Oph

The binary has been discovered by the Hipparcos satellite. It appears to be a fairly uncomplicated W-type contact binary and our solution is very well defined (Figure 2). The small value of $(M_1 + M_2)\sin^3 i = 0.487 \pm 0.009\, M_\odot$ is in accordance with the small amplitude of photometric variations (0.04 mag.), both resulting from a low inclination angle.

Our spectral type G0/1 V is in slight disagreement with the TYC2 color index of $(B-V) = 0.67$ so that some reddening of about $E_{B-V} \simeq 0.07$ is possible. The system is relatively distant (about 100 pc) and has a parallax $p = 10.09 \pm 1.22$ mas which implies $M_V = 3.53 \pm 0.27$ for the case of no reddening, while the RD97 calibration predicts $M_V(cal) = 3.79$. For $E_{B-V} = 0.07$ the absolute magnitudes would be $M_V = 3.32$ and $M_V(cal) = 3.58$, respectively.

2.9. Anon Psc = GSC 8–324

This very interesting close binary has been discovered recently by Robb et al. (1999). It does not yet have a variable star name, so we are using here an abbreviated one, GSC 8–324[5].

The system appears to be a very close pair of two detached K-type dwarfs on tight orbit with the orbital period of $P = 0.3086$ days. We included the system in our program soon after learning

[5]The name GSC 8–324 is in fact incorrect which may complicate electronic searches. It should be GSC 00008–00324. The notation used by Robb et al. (1999), who used a different numbers of leading zeros, is also incorrect.

about its discovery, led by an expectation that this is a new case of V361 Lyr-like binary which is evolving rapidly into contact (Hilditch et al. 1997), but some 4 magnitudes brighter, therefore easier for detailed studies. Recent correspondence with Dr. Robb (private communication) indicated that the spots on the surface of GSC 8–324 have moved between the seasons so that the system is *not* similar to V361 Lyr where the high stability of the accretion region strongly suggests a stable flow of matter between components. However, because the system is so very tight and yet detached – as judged by short duration of eclipses – and also relatively nearby (14 ± 8 pc, see below), it is one of the most interesting among recently discovered close binaries.

Because of the late type of the components, K4-5V (see references in Robb et al. (1999)) we feared that the magnesium triplet lines would not be as well suited for radial velocity observations as for F–G stars. For that reason we made a change in our observational setup and, in addition to the observing the same region 5185 Å as for other stars, we also obtained observations in the region centered at 5303 Å. The results of independent solutions were identical so that we made a combined solution for both spectral regions. However, we list the two series of observations separately in Table 1. The phased observations of the system are shown in Figure 3.

The radial-velocity data for the primary component are well defined for both spectral regions. In contrast, the secondary-component peaks in the broadening function are weak and the radial-velocity data are correspondingly poorer. Yet, the mass-ratio is very well determined, $q_{sp} = 0.702 \pm 0.014$. The value of $(M_1 + M_2)\sin^3 i = 1.04 \pm 0.02\,M_\odot$ together with the presence of deep eclipses suggests a possibility of a reliable combined solution for absolute elements of the system. If not for the presence of large photospheric spots, the system could serve as one of the lower main sequence calibrators.

The epoch of the superior conjunction (the primary eclipse) indicates that the orbital period could be slightly adjusted relative to the value given by Robb et al. (1999), but we leave this matter open as we cannot exclude period changes in such a short-period system.

The system was included in the Tycho-1 catalogue (HIP). The parallax has a large error, but does suggest a relatively nearby system, $p = 72 \pm 40$ mas. With the data in Robb et al. (1999), $M_V = 9.9 \pm 1.2$. The system has a large and relatively well-defined proper motion, $\mu_{RA}\cos\delta = -108.2 \pm 2.2$ mas/yr and $\mu_{dec} = -201.1 \pm 2.1$ mas/yr (TYC2), undoubtedly due to the proximity of the system.

2.10. HT Vir B

HT Vir belongs to a very close visual binary, a situation somewhat similar to that of 44 Boo, except that the separation is smaller, below one arcsec, and the brightnesses of the visual components are similar, with the contact binary being fainter only during the eclipses. We retain the designation of B for the contact system, for consistency with the previous investigations. The close visual binary is currently the subject of numerous interferometric and speckle-interferometry

studies.

The re-analysis of the Hipparcos data for visual binaries (Fabricius & Makarov 2000), gave reliable magnitudes and color indices for both components at the time that the separation was only 0.56 arcsec: $V^A = 7.80$, $(B-V)^A = 0.64$ and $V^B = 8.30$ (average magnitude), $(B-V)^B = 0.56$. Our combined spectral type, with a strong contribution of the third component, is F8V; this does not very well agree with its color index which suggests a later-type star.

HT Vir was discovered by Walker (1984) and then studied photometrically by Walker & Chambliss (1985). The photometric solution suggested that the third component provides about as much light as the eclipsing system at its light maxima. Our broadening function results confirm the strong presence of the third component; we discuss this further in Section 3. We found that the third component is in fact a radial-velocity variable with a period of 32.45 days. Thus the system is really a quadruple one, with lines of three systems visible in the spectra. We give a preliminary solution for the single-lined (SB1) system HT Vir A in Section 3 and in Table 4.

Because we have been able to isolate the signatures of HT Vir A from those of the contact binary, the radial-velocity solution for HT Vir B is very well defined (Figure 3). We note that the binary is of the A-type, yet has a surprisingly large mass ratio for such a system, $q = 0.812 \pm 0.008$. It is interesting to note that, although our determination of q for HT Vir B is the first one, Walker & Chambliss (1985) postulated a value not far from unity on the basis of the ratio of radii derived from their photometric analysis. The large mass ratio would be in accord with the relatively large amplitude of light variations of HT Vir. Walker & Chambliss (1985) estimated that $L_3/(L_{12}+L_3) \simeq 0.44$ and thus $L_3/L_{12} \simeq 0.79$ at light maxima of the close binary; HT Vir A would be then the slightly fainter of the two visual components. The light variation amplitude observed by Walker & Chambliss (1985) of about 0.42 mag., when corrected for the contribution of HT Vir A to the total systemic brightness would be then about 0.92 mag. Such a large amplitude can be generated only by a contact system with the orbit seen edge-on, but also with a mass ratio close to unity. Integrations of the individual spectral features in our broadening functions (Section 3) suggest $L_3/L_{12} \simeq 0.52 \pm 0.05$ at the light maxima of the contact system so that HT Vir A was observed by us to be fainter relative to the contact binary than before; its spectral signature was always better defined in the spectra and in the broadening functions because of its slow rotation.

The parallax of the system is the largest in this group after that of 44 Boo, $p = 15.39 \pm 2.72$ mas. With $V^B_{max} = 8.1$ and $(B-V)^B = 0.56$, this implies $M_V^B = 4.0 \pm 0.4$. The RD97 calibration predicts $M_V^B(cal) = 3.54$.

Our spectroscopic determination of T_0 shows a relatively large O–C deviation, a result of using the ephemeris of Walker & Chambliss (1985). Similarly to VZ Lib, HT Vir has not been observed for eclipse timing for a long time.

3. BROADENING FUNCTION APPROACH AND SPECTROSCOPIC COMPANIONS

3.1. Broadening functions

The spectroscopic signatures of the visual/spectroscopic companions are particularly well defined in broadening functions (BF) which give projection of a system into the velocity space (Rucinski 1999). While the close binaries of our program have short periods and thus have their rotation/revolution signatures spread over wide ranges of radial velocities, the third components – which rotate slowly – show sharp peaks in the BF. We can easily model these sharp peaks by applying the BF derivation to other sharp-line stars.

Figure 4 shows the BF's for the five triple systems, 44 Boo, V899 Her, VZ Lib, SW Lyn and HT Vir, all at phases close to orbital quadratures of the close pairs. In one case of HT Vir, we show elements of the BF decomposition into the third component and the binary itself (the last panel of Figure 4). Of particular importance is that the third component can be cleanly subtracted from the BF leaving a very well defined signature of the contact system. The success of the decomposition is due primarily to the linear properties of the BF derived through the SVD formalism (Rucinski 1999), in contrast to the cross-correlation function which is non-linear. This permits subtraction of the third component from the BF which is simple and mathematically correct. Then, through separate integration of the sharp and broad components, we can determine the brightness of the companion in relation to that of the close binary, L_3/L_{12}. Thanks to the linear SVD–BF approach, we have been able to determine radial velocities for components in close binary systems which would present totally insurmountable challenge if handled with the cross-correlation function, such as V899 Her, VZ Lib or SW Lyn.

The linear deconvolution technique that we use to obtain the broadening functions is not the only one available for determination of accurate radial velocities from blended spectra showing lines of several components. In recent years, a powerful technique called TODCOR has been developed for close binaries by Zucker & Mazeh (1994) and then extended into the case of triple-lined systems by Zucker et al. (1995); the latter modification has been already successfully applied in some difficult cases of multi-lined systems (Jha et al. 2000). We did not use this technique for the several reasons. Not only that we feel more comfortable with a tool developed by ourselves, but (1) so far, TODCOR has not been demonstrated to work for very broad lines of contact binaries, and (2) our case of mixed very broad and narrow spectral signatures is even more difficult and would require even more extensive testing. We fear in particular that the non-linear nature of the cross-correlation would complicate derivation of relative brightnesses of components for systems with components showing very different degrees of rotational broadening.

In three (V899 Her, SW Lyn, HT Vir), possibly four (VZ Lib), among the triple-lined systems, the third component appears to be a radial-velocity variable. We will comment on each system in the separate subsections below.

3.2. 44 Boo A

The observations lasted too short in the case of 44 Boo A to note any long-term radial-velocity changes. However, since we wanted to obtain the best radial-velocity data for the close binary 44 Boo B, the presence of the bright companion did require some additional precautions. In particular, an attempt was made during the observations to place the brighter component 44 Boo A as much outside the spectrograph slit as possible. The separation is currently about 1.7 arcsec so that it is comparable to the width of our slit (1.8 arcsec), which cannot be rotated. Because the component A is about 1.8 times brighter than B (Hill et al. 1989) and its lines are sharp and very well defined, its signature is always visible in the BF (first panel of Figure 4). By attempting to place its image outside the slit, we partly succeeded in suppressing its contribution (to the level $L_3/L_{12} \simeq 0.4 - 0.7$ depending on the seeing, as measured in the broadening functions), but we did not eliminate it totally achieving only modification of its relative intensity in the BF. Its radial velocity derived from the BF is also incorrect (by up to 12 km s^{-1}) because the light was spilling over always from one side of our relatively wide slit. To derive an unbiased velocity of 44 Boo, we made three additional observations of this component at the slit center and measured the velocity of this component separately. Its average velocity for the epoch JD(hel) = 2,450,945.996 is $V^A = -34.93 \pm 0.64$. The detailed data are given in Table 3.

3.3. V899 Her A

There exist no earlier reports of the presence of a third component in this star which has been only recently discovered as a variable star. As we can see in the second top panel of Figure 4, the third component dominates the broadening function of V899 Her, so we call it the component A. The ratio of brightnesses at phases close to orbital quadratures is $L_3/L_{12} = 1.5 \pm 0.1$. The spectrum of the system, F5 V, is also dominated by this component and we see only weak signatures of the broadened G-type spectrum in the BF. Only thanks to the linearity of the broadening function determination we have been able to study this interesting system.

We found that V899 Her A slowly changes its radial velocity. These variations are not reflected in the systemic velocity of the close pair, so that the companion A itself is probably a wide spectroscopic binary. The radial-velocity data for V899 Her A are shown in Figure 5. We had many observations for this star so that we could group them into nightly average values. These in turn permitted us to obtain independent estimates of measurement errors for individual observations, after all stages of the combined standard and broadening-function processing and component separation. For such a sharp-line star, the errors of the nightly averages are small at a level typically 0.5 to 1.0 km s^{-1}.

3.4. VZ Lib B

We have detected a spectroscopic companion of VZ Lib. The broadening function (the left lower panel in Figure 4) indicates that in this case the brightness of the companion is lower that that of the close binary, $L_3/L_{12} = 0.20 \pm 0.04$. Because the close binary has a relatively small mass ratio, the BF peak of the third star is usually merged with the broadening lobe of the primary, more massive component of the W UMa-type system of VZ Lib.

The radial velocities of the third component show a nightly spread of 2.6 to 4.3 km s^{-1}, whereas errors for sharp line stars are typically ≤ 1 km s^{-1}. This may be an indication that the spectroscopic companion is itself a close binary although we found that derivation of the velocities for all three stars in this case was very difficult because of the relative faintness of the system and extensive blending of the components in the broadening function. The variations of the third component appear to be slow (Figure 5), but may result from grouped sampling of more rapid changes. The system requires further radial-velocity observations to confirm that the companion has variable radial velocity and that the system is actually a quadruple one.

3.5. SW Lyn B

We have detected a third star in the system of SW Lyn. It is well visible in the broadening function in Figure 4 (middle lower panel). As mentioned in the description of the close binary in Section 2, the presence of the signal from the third star as well as the dominant role of the massive and bright primary component of the Algol system resulted in difficulties with the radial-velocity measurements of the secondary star of the close system.

The third star in SW Lyn is moderately bright, $L_3/L_{12} = 0.33 \pm 0.05$ (for the contact system at the orbital quadrature), and is a radial-velocity variable so that the whole system is a quadruple one. The radial-velocity changes of the third component are slow and certainly compatible with the orbital period of 2128 day which is noticeable in the eclipse timing for the close pair (Ogłoza et al. 1998). However, we see no direct indication that this is the same star. Unfortunately, contrary to V899 Her or VZ Lib, we have been unable to check if seasonal data would give the complementary systemic velocity variation for the close pair; we could only solve the second season or all the data together. As we described in Section 2 the orbital solutions for the close pair based on all the observations from both seasons and, separately, on the observations from the second season, gave identical sets of orbital parameters (within the errors). This would suggest that the spectroscopic companion and the eclipse-timing perturber are not the same object.

3.6. HT Vir A

HT Vir has been known as a close visual binary with a separation of less than one arcsec (Walker 1984; Walker & Chambliss 1985). In terms of the overall properties, the system is somewhat similar to 44 Boo. Walker & Chambliss (1985) determined that the component A had brightness comparable to that of the close binary ($L_3/L_{12} \simeq 0.79$) and was slightly fainter of the two even at light maxima of the contact system. By integration of the separate components of the broadening function (upper right panel in Figure 4), we obtained $L_3/L_{12} \simeq 0.52 \pm 0.05$, so that we found that HT Vir A was about two times fainter than the contact binary at its light maxima. In fact, we derived the ratio of the luminosities to be about 0.48 ± 0.03 for phases around 0.25 and about 0.56 ± 0.03 for phases around 0.75; this may reflect either an asymmetry in the light maxima of HT Vir B or systematic errors in our estimates of L_3/L_{12} for the mutually oppositely-orientated peaks in the broadening function. After subtraction of the scaled peak of the third component, we obtained an excellent radial-velocity orbit for HT Vir B (as described in Section 2).

We discovered that HT Vir A is a relatively close, single-lined (SB1) binary so that the HT Vir system is a quadruple one. The data for this star showed a scatter of about 20 km s^{-1} which we analyzed for periodicity. Solution of the radial-velocity data, using the program of Morbey (1975), with a preliminary orbital period of 32.45 days, leads to an eccentric orbit with parameters listed in Table 4. We show the solution for HT Vir A in the last panel of Figure 5.

4. SUMMARY

The paper brings radial-velocity data and orbital solutions for the fourth group of ten close binary systems that we observed at the David Dunlap Observatory. Only 44 Boo and SW Lyn have been observed spectroscopically before; for both, we provide much improved spectroscopic orbits. All systems are double-lined (SB2) binaries with visible spectral lines of both components. We give the values of $(M_1 + M_2) \sin^3 i = 1.0385 \times 10^{-7} \, (K_1 + K_2)^3 \, P(\mathrm{day}) \, M_\odot$ in Table 2. As in the previous papers of this series, we have not been able to converted them into the sums of masses because in most cases the inclination angle is either unknown or not trustworthy. We note that the photometric discoveries of the Hipparcos project (FI Boo, V2150 Cyg, EX Leo, V2377 Oph) tend to have small values of $(M_1 + M_2) \sin^3 i$, in accord with their small photometric amplitudes, both features apparently due to low orbital inclinations. But we also found that some of the newly-discovered systems may have small photometric amplitudes because of the dilution of light in a triple system; the perfect example is V899 Her. By discovering low photometric amplitude binary systems, the Hipparcos mission has therefore contributed substantially to rectifying the statistics of bright contact binaries; this statistics had been known to be skewed toward large amplitude variables (Rucinski & Kałużny 1994; Rucinski 1997).

Five system in the current group are members of close visual and/or spectroscopic triple-lined systems (44 Boo, V899 Her, VZ Lib, SW Lyn, HT Vir); among them three and possibly

four companions are themselves close binaries. We have been able to provide good data for these systems mostly because of the superior capabilities of the linear SVD broadening-function approach (Rucinski 1999) in resolving individual components in the triple-lined spectra.

The authors would like to thank Jim Thomson for help with observations, Dr. Frank Fekel for providing us a list of early-type standard stars and Dr. Russ Robb for correspondence about GSC 8–324. We thank the referee for a careful and constructive review.

The visit of WO to the David Dunlap Observatory was possible thanks to support from Professor Bohdan Paczynski, through the Polish Astronomical Foundation. Support from the Natural Sciences and Engineering Council of Canada to SMR is acknowledged with gratitude.

The research has made use of the SIMBAD database, operated at the CDS, Strasbourg, France and accessible through the Canadian Astronomy Data Centre, which is operated by the Herzberg Institute of Astrophysics, National Research Council of Canada.

REFERENCES

Abt, H. A. 1981, ApJS, 45, 437

Claria, J. J. & Lapasset, E. 1981, Inf. Bull. Variable Stars, No.2035

Duerbeck, H. W. 1997, Inf. Bull. Variable Stars, No.4513

European Space Agency. 1997. The Hipparcos and Tycho Catalogues (ESA SP-1200)(Noordwijk: ESA) (HIP)

Fabricius, C. & Makarov, V. V. 2000, A&A, 356, 141

Grenier, S., Baylac, M.-O., Rolland, L., Burnage, R., Arenou, F., Briot, D., Delmas, F., Duflot, M., Genty, V., Gomez, A.E., Halbwachs, J.-L., Marouard, M., Oblak, E. & Sellier, A. 1999, A&A, 137, 451

Hilditch, R. W., Collier Cameron, A., Hill, G., Bell, S. A. & Harries, T. J. 1997, MNRAS, 291, 749

Hill, G., Fisher, W. A. & Holmgren, D. 1989, A&A, 211, 81

Hoffmeister, C. 1949, Erg. AN, 12, 1, 21

Hog, E., Fabricius, C., Makarov, V. V., Urban, S., Corbin, T., Wycoff, G., Bastian, U., Schwekendiek, P. & Wicenec, A. 2000, A&A, 355, L27 (TYC2)

Jha, S., Torres, G., Stefanik, R. P., Latham, D. W. & Mazeh, T. 2000, MNRAS, 317, 375

Lu, W., & Rucinski, S. M. 1993, AJ, 106, 361

Lu, W., & Rucinski, S. M. 1999, AJ, 118, 515 (Paper I)

Morbey, C. 1975, PASP, 87, 689

Ogłoza, W., Zoła, S., Tremko, J. & Kreiner, J. M. 1998, A&A, 340, 81

Ogłoza, W., Dróżdż, M. & Zoła, S. 2000, Inf. Bull. Variable Stars, No.4877

Robb, R. M., Wagg, J., Berndsen, A. & Desroches, L. 1999, Inf. Bull. Variable Stars, No.4800

Rucinski, S. M. 1992, AJ, 104, 1968

Rucinski, S. M. 1994, PASP, 106, 462

Rucinski, S. M. 1997, AJ, 113, 1112

Rucinski, S. M. 1999, "Precise Stellar Radial Velocities", ASP Conf. Ser. Vol.185, eds. J. B. Hearnshaw & C. D. Scarfe, p.82

Rucinski, S.M., & Duerbeck, H.W. 1997, PASP, 109, 1340 (RD97)

Rucinski, S. M. & Kałużny, J. 1994, MSAIt, 65, 113

Rucinski, S. M. & Lu, W. 1999, AJ, 118, 2451 (Paper II)

Rucinski, S. M., Lu, W. & Shi, J. 1993, AJ, 106, 1174

Rucinski, S. M., Lu, W. & Mochnacki, S. W. 2000, AJ, 120, 1133 (Paper III)

Schilt, J. 1926, ApJ, 64, 215

Tsesevich, B. P. 1954, Izv. Astr. Obs. Odessa, 4, 196

Vetešnik, M. 1968, Bull. Astr. Inst. Czechoslovakia, 19, 110

Vetešnik, M. 1977, Bull. Astr. Inst. Czechoslovakia, 28, 120

Walker, R. L. 1984, Inf. Bull. Variable Stars, No.2486

Walker, R. L. & Chambliss, C. R. 1985, AJ, 90, 346

Zucker, S. & Mazeh, T. 1994, ApJ, 420, 806

Zucker, S., Torres, G. & Mazeh, T. 1995, ApJ, 452, 863

Errata to Paper II:

This preprint was prepared with the AAS LaTeX macros v5.0.

The residuals ΔV listed in Table 1 for SV Equ are incorrect and do not agree with Figure 1 and the quoted value of the error per single observations, as given in Table 2. The correct residuals can be computed from the original data and the spectroscopic elements.

Captions to figures:

Fig. 1.— Radial velocities of the systems 44 Boo B, FI Boo, V2150 Cyg and V899 Her B are plotted in individual panels versus orbital phases. The lines give the respective circular-orbit (sine-curve) fits to the radial velocities. 44 Boo B and FI Boo are W-type systems while V2150 Cyg and V899 Her B are A-type systems. Short marks in the lower parts of the panels show phases of available observations which were not used in the solutions because of the blending of lines. Open symbols in this and the next two figures indicate observations given half-weights in the solutions. All panels have the same vertical scales.

Fig. 2.— Radial velocities of the systems EX Leo, VZ Lib A, SW Lyn A and V2377 Oph. Only V2377 Oph is a W-type system. SW Lyn A is most probably a short-period Algol system and EX Leo and VZ Lib A are contact systems of the A-type.

Fig. 3.— Radial velocities of the systems GSC 8-324 and HT Vir B. The first is a very close, but detached or semi-detached system, while HT Vir B is a contact A-type system with a surprisingly large mass-ratio.

Fig. 4.— The broadening functions for five close binary systems with spectroscopic companions. For HT Vir, we show (1) the full broadening function with the signature of a sharp-line template shifted for clarity by 100 km $^{-1}$ (dotted line in the right upper panel, shifted to right for clarity) and (2) the same function with the sharp-line component subtracted, leaving only the signature of the contact binary HT Vir B (right lower panel). In each panel the number gives the orbital phase selected to be close to the orbital quadrature.

Fig. 5.— The radial-velocity variations of the spectroscopic companions of V899 Her A, VZ Lib B, SW Lyn B and HT Vir A. For HT Vir A we show the radial-velocity data phased with period of 32.45 days together with our preliminary single-line orbital solution. The vertical scale in all panels has the same span of 60 km s^{-1}, but the time axis is different for each panel.

Table 1. DDO observations of the fourth group of ten close binary systems

HJD–2,400,000	Phase	V_1	ΔV_1	V_2	ΔV_2
44 Boo B					
50939.6513	0.1943	91.3	3.3	−241.5	−6.3
50939.6543	0.2055	92.5	2.1	−243.7	−3.5
50939.6572	0.2164	94.5	2.2	−246.6	−2.5
50939.6602	0.2276	89.7	−4.0	−247.8	−0.9
50939.6631	0.2384	94.6	0.1	−249.8	−1.2
50939.6661	0.2496	93.2	−1.6	−247.5	1.7
50939.6713	0.2690	92.9	−1.1	−251.4	−3.8
50939.6742	0.2798	90.0	−2.8	−246.9	−1.8
50939.6771	0.2907	87.7	−3.5	−241.2	0.5
50939.6801	0.3019	87.3	−1.6	−239.5	−2.5
50939.6830	0.3127	83.0	−3.2	−230.8	0.7
50939.6860	0.3239	78.9	−4.0	−226.4	−1.7
50939.6889	0.3347	78.0	−1.2	−219.0	−1.8
50939.6932	0.3508	70.0	−3.0	−205.2	−0.8
50939.6962	0.3620	65.2	−2.8	−190.9	3.4
50939.6991	0.3728	63.2	0.3	−181.8	1.9
50939.7020	0.3836	67.7	10.3	−171.1	1.2
50939.7050	0.3948	59.2	7.9	−155.0	4.8
50939.7079	0.4057	50.3[b]	···	−143.9[b]	···
50939.7109	0.4169	···	···	···	···
50939.7158	0.4352	···	···	···	···
50939.7187	0.4460	···	···	···	···
50939.7216	0.4568	···	···	···	···
50939.7246	0.4680	···	···	···	···
50939.7275	0.4789	···	···	···	···
50939.7305	0.4901	···	···	···	···
50939.7334	0.5009	···	···	···	···
50939.7379	0.5177	···	···	···	···
50939.7408	0.5285	···	···	···	···
50939.7438	0.5397	···	···	···	···
50939.7467	0.5506	···	···	···	···
50939.7496	0.5614	···	···	···	···
50939.7526	0.5726	···	···	···	···
50939.7555	0.5834	−79.6[b]	···	96.1[b]	···
50939.7624	0.6092	−89.3	−0.0	129.9	1.3
50939.7653	0.6200	−101.9	−6.9	139.8	−0.6
50939.7683	0.6312	−103.5	−2.9	149.7	−2.2
50939.7712	0.6420	−110.4	−4.8	161.8	−0.4
50939.7741	0.6529	−109.8	0.5	178.7	7.1
50939.7771	0.6641	−115.8	−1.2	181.7	1.2
50939.7800	0.6749	−120.5	−2.2	188.6	0.5

Table 1—Continued

HJD–2,400,000	Phase	V_1	ΔV_1	V_2	ΔV_2
50939.7844	0.6913	−126.9	−3.9	195.3	−2.6
50939.7874	0.7025	−125.8	−0.2	199.8	−3.4
50939.7903	0.7133	−128.1	−0.5	203.3	−4.0
50939.7933	0.7246	−127.4	1.8	206.3	−4.2
50939.7962	0.7354	−126.1	4.0	204.5	−7.9
50939.7991	0.7462	−133.3	−2.7	206.3	−7.0
50939.8021	0.7574	−131.3	−0.8	207.4	−5.8
50939.8081	0.7798	−130.7	−2.1	203.0	−6.4
50939.8110	0.7906	−127.1	−0.2	197.7	−8.2
50939.8140	0.8018	−127.7	−3.0	196.9	−4.3
50939.8169	0.8127	−125.4	−3.4	193.0	−2.7
50939.8199	0.8239	−118.6	0.1	187.9	−1.0
50939.8228	0.8347	−114.7	0.3	186.0	4.6
50939.8257	0.8455	−107.6	3.3	181.8	8.8
50939.8304	0.8631	−95.8	7.5	161.2	3.8
50939.8333	0.8739	−95.5	2.6	153.7	6.9
50939.8363	0.8851	−86.4	6.0	144.0	9.0
50939.8392	0.8959	−85.6	0.8	134.2	11.4
50939.8422	0.9071	−75.9	4.1	···	···
50939.8451	0.9180	−71.6[b]	···	···	···
50939.8481	0.9292	···	···	···	···
50939.8529	0.9471	···	···	···	···
50939.8559	0.9583	···	···	···	···
50939.8588	0.9691	···	···	···	···
50939.8618	0.9803	···	···	···	···
50939.8647	0.9911	···	···	···	···
50939.8676	0.0020	···	···	···	···
50939.8706	0.0132	···	···	···	···
50939.8749	0.0292	···	···	···	···
50939.8779	0.0404	···	···	···	···
50939.8808	0.0513	···	···	···	···
50940.6688	0.9936	···	···	···	···
50940.6722	0.0063	···	···	···	···
50940.6751	0.0171	···	···	···	···
50940.6781	0.0283	···	···	···	···
50940.6810	0.0391	···	···	···	···
50940.6839	0.0499	···	···	···	···
50940.6869	0.0611	34.4[b]	···	−127.9[b]	···
50940.6911	0.0768	45.0[b]	···	−139.0[b]	···
50940.6940	0.0877	51.7	10.6	−142.5[b]	···
50940.6970	0.0989	48.2	0.5	−151.9	0.6
50940.6999	0.1097	53.6	−0.2	−167.9	−2.9

Table 1—Continued

HJD–2,400,000	Phase	V_1	ΔV_1	V_2	ΔV_2
50940.7029	0.1209	59.2	−0.5	−178.5	−1.3
50940.7058	0.1317	66.3	1.2	−186.6	1.6
50940.7087	0.1425	73.5	3.4	−195.5	3.0
50940.7144	0.1638	80.2	1.5	−209.3	6.8
50940.7173	0.1747	81.3	−1.1	−227.7	−3.9
50940.7202	0.1855	86.6	0.9	−233.6	−3.1
50940.7232	0.1967	89.8	1.3	−239.3	−3.0
50940.7261	0.2075	91.1	0.3	−242.0	−1.0
50940.7291	0.2187	88.7	−3.9	−243.0	1.7
50940.7320	0.2295	89.5	−4.4	−244.9	2.4
50940.7351	0.2411	92.5	−2.1	−246.1	2.7
50948.6702	0.8698	−97.0	3.1	159.8	8.9
50949.6796	0.6388	−107.5	−3.3	164.4	5.2
FI Boo					
51649.8575	0.2617	23.8	−1.1	−177.0	1.5
51649.8661	0.2838	21.1	−2.7	−165.2	10.4
51649.8747	0.3058	19.9	−1.8	−167.5	2.4
51649.8852	0.3328	10.7	−7.0	−161.2	−1.9
51662.5589	0.8296	−83.4	−4.6	99.7	−0.5
51662.5668	0.8498	−84.0	−9.0	90.8	0.7
51662.5742	0.8688	−74.9	−4.1	80.3	1.4
51662.5830	0.8914	−68.2	−3.1	66.5	3.0
51662.5907	0.9111	−75.7	−16.2	39.4	−9.1
51662.6065	0.9516	···	···	···	···
51662.6170	0.9786	···	···	···	···
51662.6251	0.9993	···	···	···	···
51662.6330	0.0196	···	···	···	···
51662.6438	0.0473	···	···	···	···
51662.6517	0.0675	···	···	···	···
51662.6624	0.0950	···	···	···	···
51662.6703	0.1152	0.2	−6.2	−133.1	−4.4
51662.6779	0.1347	10.5	−0.6	−142.8	−1.2
51662.6870	0.1581	15.8	−0.3	−155.7	−0.9
51662.6949	0.1783	22.8	3.3	−161.2	2.9
51662.7030	0.1991	22.7	0.5	−169.4	2.0
51662.7125	0.2234	25.0	0.7	−174.4	2.4
51662.7203	0.2434	25.3	0.3	−175.3	3.5
51662.7281	0.2634	22.6	−2.2	−178.4	−0.0
51662.8284	0.5206	···	···	···	···
51662.8367	0.5419	···	···	···	···
51662.8445	0.5619	···	···	···	···
51662.8540	0.5863	···	···	···	···

Table 1—Continued

HJD–2,400,000	Phase	V_1	ΔV_1	V_2	ΔV_2
51662.8619	0.6065	...	...	...	...
51662.8698	0.6268	−75.2	−5.4	72.2	−3.8
51662.8799	0.6527	−78.4	−2.9	91.8	0.3
51662.8877	0.6727	−77.6	1.5	104.2	3.0
51664.6906	0.2955	20.8	−2.0	−171.9	1.0
51664.7008	0.3217	16.9	−2.6	−161.6	2.5
51664.7115	0.3491	15.3	0.7	−145.5	5.5
51664.7223	0.3768	7.5	−0.9	−132.9	1.3
51664.7769	0.5168	...	...	...	...
51664.7419	0.4271	...	...	...	...
51664.7506	0.4494	...	...	...	...
51664.7594	0.4719	...	...	...	...
51664.7769	0.5168	...	...	...	...
51786.5361	0.7215	−83.2	1.4	124.6	8.6
51786.5614	0.7863	−80.8	3.3	119.7	5.2
51786.5699	0.8081	−78.3	3.6	113.3	4.7
51786.5796	0.8330	−74.2	4.0	111.5	12.9
V2150 Cyg					
50949.8540	0.5075	...	...	...	...
50949.8634	0.5234	...	...	...	...
50949.8733	0.5401	...	...	...	...
51459.6026	0.7789	113.4	2.9	−162.5	4.2
51459.6132	0.7968	108.2	1.0	−158.5	4.0
51459.6250	0.8167	103.4	1.7	−151.7	4.0
51459.6357	0.8348	99.6	4.4	−148.0	−0.5
51459.6484	0.8562	91.8	6.1	−134.0	1.6
51459.6594	0.8748	79.2	3.2	−122.1	1.4
51664.7869	0.4583	...	...	...	...
51664.7940	0.4703	...	...	...	...
51664.8017	0.4833	...	...	...	...
51664.8097	0.4968	...	...	...	...
51664.8195	0.5134	...	...	...	...
51664.8276	0.5271	...	...	...	...
51664.8356	0.5406	...	...	...	...
51664.8469	0.5597	...	...	...	...
51664.8550	0.5733	...	...	...	...
51664.8630	0.5869	...	...	...	...
51664.8726	0.6031	58.5	−4.4	−117.9[a]	−10.7
51664.8804	0.6163	66.6	−4.3	−128.5	−11.3
51668.7676	0.1841	−126.8	0.8	128.6	−1.8
51668.7784	0.2023	−133.5	−0.8	128.0	−8.6
51668.7911	0.2238	−135.8	0.7	135.8	−5.7

Table 1—Continued

HJD–2,400,000	Phase	V_1	ΔV_1	V_2	ΔV_2
51668.8021	0.2424	−138.8	−0.7	137.5	−5.9
51668.8123	0.2596	−138.2	−0.2	142.3	−1.0
51668.8196	0.2719	−136.9	0.2	137.5	−4.6
51668.8273	0.2849	−134.3	0.9	134.2	−5.6
51668.8394	0.3054	−135.6	−4.9	131.6	−2.6
51670.7659	0.5604	...	...	...	...
51670.7766	0.5785	...	...	...	...
51670.7879	0.5976	49.1	−10.2	−120.3[a]	−17.5
51670.7975	0.6138	67.4	−2.0	−126.2	−10.8
51670.8085	0.6324	83.5	3.6	−129.5	−1.1
51670.8172	0.6471	88.4	1.1	−143.9	−6.3
51670.8258	0.6616	95.7	1.9	−148.9	−3.2
51670.8372	0.6809	103.2	2.2	−157.0	−2.3
51670.8460	0.6957	108.1	2.7	−160.5	−0.3
51670.8550	0.7109	112.4	3.6	−168.3	−3.8
51671.7948	0.2988	−134.9	−2.5	142.5	6.2
51671.8036	0.3137	−126.1	2.2	134.4	3.2
51671.8122	0.3282	−126.9	−3.5	129.1	4.0
51671.8224	0.3455	−111.7	4.6	119.4	3.1
51671.8310	0.3600	−108.3	1.2	110.5	2.8
51671.8396	0.3745	−102.9	−1.1	105.6	7.5
51671.8580	0.4056	−78.0	4.9	85.0[a]	10.4
51671.8666	0.4201	...	...	...	...
51671.8752	0.4347	...	...	...	...
51785.6699	0.7022	103.9	−3.1	−166.6	−4.4
51785.6806	0.7203	107.7	−2.7	−164.6	1.9
51785.6922	0.7399	110.2	−2.2	−170.2	−1.3
51785.7028	0.7578	116.8	4.3	−166.0	3.0
51785.7132	0.7754	113.8	2.8	−160.7	6.5
51822.6082	0.1132	−91.0	3.7	91.8	2.5
51822.6168	0.1277	−107.0	−4.0	97.8	−1.8
51822.6264	0.1439	−107.9	3.5	109.9	−0.2
51822.6349	0.1583	−114.8	3.2	117.9	−0.4
51822.6435	0.1728	−121.5	2.3	127.5	2.0
51822.6533	0.1894	−125.7	3.6	133.6	1.2
51822.6620	0.2041	−128.6	4.5	136.6	−0.5
51822.6707	0.2188	−134.4	1.4	137.0	−3.6
V899 Her B					
51402.5597	0.2971	−135.8	11.1	211.6	−1.5
51402.5671	0.3146	−129.2	12.6	204.6	0.6
51402.5745	0.3322	−134.3	0.8	173.2	−19.0
51402.5827	0.3517	−127.4	−1.4	164.1	−12.1

Table 1—Continued

HJD–2,400,000	Phase	V_1	ΔV_1	V_2	ΔV_2
51402.5908	0.3709	−118.7	−3.3	154.6	−2.9
51402.5987	0.3897	−114.6	−10.9	130.2	−6.6
51402.6073	0.4101	−119.0	−29.4	114.7	2.8
51402.6147	0.4276	−118.2[a]	−41.6	102.2[a]	13.5
51456.5091	0.3903	−122.0	−18.7	99.0	−37.1
51456.5197	0.4154	−118.5[a]	−32.8	97.1[a]	−7.9
51456.5328	0.4465	···	···	···	···
51456.5437	0.4724	···	···	···	···
51456.5518	0.4916	···	···	···	···
51466.4905	0.0893	···	···	···	···
51466.4977	0.1064	−125.9	−24.8	130.8	−1.4
51466.5049	0.1235	−125.6	−13.5	145.3	−6.2
51466.5130	0.1427	−122.2	0.9	164.2	−6.8
51466.5201	0.1596	−142.6	−11.1	187.6	1.8
51466.5273	0.1767	−141.6	−3.0	192.7	−5.8
51466.5354	0.1959	−143.3	1.7	175.4	−34.4
51466.5464	0.2220	−137.0	13.7	210.0	−9.9
51466.5540	0.2401	−118.8	33.8	227.3	4.2
51466.5621	0.2593	−148.9	3.7	238.3	15.1
51634.7840	0.6721	118.0	14.8	−237.9	−8.8
51634.7946	0.6973	120.6	8.9	−241.8	2.4
51634.8066	0.7258	126.4	8.8	−253.8	0.7
51634.8173	0.7512	118.2	−0.9	−244.2	13.1
51634.8294	0.7799	119.7	3.0	−256.1	−3.1
51634.8401	0.8053	101.8	−9.2	−244.6	−1.7
51634.8639	0.8619	84.8	−2.1	−206.5	−6.2
51634.8746	0.8873	91.2	19.6	−180.6	−7.3
51634.8871	0.9169	79.2[a]	28.3	−135.6	1.1
51635.8276	0.1500	−110.2	16.6	168.0	−9.6
51635.8386	0.1761	−109.8	28.6	179.8	−18.3
51635.8494	0.2017	−129.0	17.6	226.4	13.8
51635.8709	0.2528	−143.5	9.3	246.8	23.3
51635.8819	0.2789	−131.2	19.4	249.7	30.1
51635.8937	0.3069	−134.9	9.3	251.1	42.7
51635.9051	0.3340	−102.4	31.9	220.8	29.9
51647.7633	0.4892	···	···	···	···
51647.7712	0.5079	···	···	···	···
51647.7786	0.5255	···	···	···	···
51647.7859	0.5428	···	···	···	···
51647.7972	0.5697	···	···	···	···
51647.8045	0.5870	···	···	···	···
51647.8119	0.6046	93.2[a]	27.0	−189.7	−26.0

Table 1—Continued

HJD–2,400,000	Phase	V_1	ΔV_1	V_2	ΔV_2
51647.8225	0.6297	98.2	16.1	−196.2	−4.4
51647.8298	0.6471	103.8	12.1	−216.6	−7.9
51647.8375	0.6653	112.6	12.3	−232.1	−8.1
51647.8487	0.6919	120.5	10.3	−246.8	−5.4
51647.8560	0.7093	116.3	1.6	−255.5	−6.1
51647.8632	0.7264	116.8	−0.8	−258.8	−4.2
51647.8737	0.7513	123.4	4.3	−254.4	2.9
51647.8810	0.7686	117.1	−1.1	−255.0	0.6
51647.8882	0.7857	111.0	−4.7	−247.4	3.8
51663.5826	0.0493	...	...	...	...
51663.5932	0.0744	...	...	...	...
51663.6068	0.1067	−123.0	−21.7	122.8	−9.8
51663.6182	0.1338	−132.6	−14.4	150.9	−11.4
51663.6307	0.1635	−141.4	−8.2	178.3	−10.6
51663.6414	0.1889	−145.1	−2.2	195.4	−10.7
51663.6535	0.2176	−149.1	0.9	207.9	−10.7
51663.6642	0.2430	−152.3	0.4	222.5	−0.8
51663.6774	0.2744	−152.8	−1.6	198.4	−22.4
51663.6884	0.3005	−142.0	4.0	217.9	6.3
EX Leo					
51570.7937	0.3369	−52.2	2.7	210.7	1.3
51570.8051	0.3648	−44.4	5.2	191.4	8.7
51570.8185	0.3976	−32.6	9.2	174.0	30.3
51570.8325	0.4318	...	...	...	...
51570.8435	0.4587	...	...	...	...
51570.8550	0.4869	...	...	...	...
51570.8626	0.5055	...	...	...	...
51570.8698	0.5231	...	...	...	...
51570.8879	0.5674	...	...	...	...
51570.8952	0.5853	21.4	6.3	...	...
51570.9024	0.6029	26.9	7.1	−183.5	−17.0
51570.9123	0.6271	29.5	3.8	−207.1	−11.2
51570.9195	0.6447	28.2	−1.2	−223.6	−9.0
51570.9267	0.6624	35.9	3.3	−235.3	−4.4
51570.9373	0.6883	44.1	7.7	−246.5	3.4
51570.9445	0.7059	33.4	−4.9	−265.7	−6.5
51570.9517	0.7235	37.0	−2.5	−262.3	3.2
51648.6145	0.7922	40.0	1.6	−253.7	6.3
51648.6232	0.8135	33.2	−3.0	−243.6	5.2
51648.6330	0.8374	30.0	−2.7	−232.4	−1.3
51648.6415	0.8583	21.2	−7.6	−211.2	0.4
51648.6524	0.8849	18.0	−4.9	−199.8	−18.0

Table 1—Continued

HJD–2,400,000	Phase	V_1	ΔV_1	V_2	ΔV_2
51648.6609	0.9057	...	...	...	...
51648.6705	0.9292	...	...	...	...
51648.6790	0.9500	...	...	...	...
51648.6904	0.9779	...	...	...	...
51648.6994	1.0000	...	...	...	...
51648.7086	0.0225	...	...	...	...
51648.7298	0.0744	...	...	...	...
51648.7383	0.0952	−45.2	−5.3	131.7	−2.4
51648.7468	0.1160	−51.3	−6.1	172.2	11.5
51648.7568	0.1404	−52.5	−1.8	193.9	5.8
51648.7654	0.1615	−55.4	−0.8	209.5	1.5
51648.7739	0.1823	−61.2	−3.4	226.0	2.1
51648.7848	0.2090	−58.1	2.6	233.0	−5.4
51648.7933	0.2298	−69.1	−7.2	238.9	−5.9
51648.8020	0.2511	−67.3	−5.0	243.2	−3.7
51659.6067	0.6940	35.5	−1.6	−252.2	1.0
51659.6195	0.7253	37.8	−1.8	−263.6	2.3
51659.6335	0.7596	36.0	−4.1	−259.0	9.6
VZ Lib A					
50520.8497	0.3714	−116.5	−35.8	182.8	4.8
50520.8605	0.4016	−114.2	−43.3	152.5	15.9
50520.8727	0.4356	...	...	...	...
50520.8835	0.4658	...	...	...	...
50520.8970	0.5034	...	...	...	...
50520.9095	0.5383	...	...	...	...
50520.9229	0.5757	...	...	...	...
50520.9338	0.6062	7.5	−3.8	−192.2[a]	17.9
50539.9024	0.5522	...	...	...	...
50540.7525	0.9250	25.4	25.4	−205.6[a]	−43.2
50540.7632	0.9549	...	...	...	...
50540.7754	0.9889	...	...	...	...
50540.7871	0.0216	...	...	...	...
50540.8005	0.0590	...	...	...	...
50540.8113	0.0891	−54.6[a]	12.9	151.2[a]	28.6
50540.8235	0.1232	−76.9	2.1	144.6	−26.5
50541.8017	0.8536	36.2	12.8	−277.0	−15.8
50541.8124	0.8835	25.7	11.0	−264.8	−40.3
50541.8246	0.9175	14.8[a]	12.0	−232.6[a]	−58.2
50596.6337	0.9032	2.8	−5.3	−240.9	−44.5
50596.6445	0.9333	...	...	...	...
50596.6571	0.9685	...	...	...	...
50596.6678	0.9984	...	...	...	...

Table 1—Continued

HJD–2,400,000	Phase	V_1	ΔV_1	V_2	ΔV_2
50596.6799	0.0321	...	...	...	...
50596.6905	0.0617	...	...	...	...
50930.7689	0.5566	...	...	...	...
50930.7796	0.5864	2.5	−1.8	−216.2[a]	−35.6
50930.7916	0.6199	17.3	1.5	−263.3	−34.3
50930.8029	0.6515	39.8	15.1	−256.9	9.8
50930.8150	0.6852	36.3	4.5	−282.4	14.3
51254.8413	0.1222	−86.8	−8.1	180.9	11.1
51254.8521	0.1523	−66.7	20.5	211.0	5.6
51254.8667	0.1931	−83.4	11.9	217.7	−22.1
51254.8775	0.2232	−133.0	−34.3	235.0	−19.1
51281.7208	0.1495	−87.7	−1.3	237.8	35.5
51281.7321	0.1810	−101.4	−8.1	253.2	21.8
51281.7443	0.2151	−107.5	−9.5	234.1	−17.1
51281.7552	0.2455	−100.0	−0.4	275.2	17.2
51281.7690	0.2840	−107.8	−9.7	242.2	−9.4
51281.7808	0.3170	−72.7	21.0	253.2	20.3
51281.7935	0.3524	−56.8	29.2	207.5	7.2
51281.8045	0.3831	−53.5	23.6	153.4	−9.3
51281.8177	0.4200	−54.3	9.9	147.3[a]	39.0
51281.8295	0.4529	...	...	...	...
51281.8424	0.4889	...	...	...	...
51281.8536	0.5202	...	...	...	...
51281.8667	0.5567	...	...	...	...
51281.8779	0.5880	...	...	...	...
51281.8906	0.6234	43.1	26.2	−249.2	−15.6
51281.9021	0.6555	24.7	−1.0	−281.5	−10.6
51297.7375	0.8560	30.4	7.6	−229.3	29.2
51297.7484	0.8864	30.0	16.3	−184.4	36.0
51297.7602	0.9194	31.3[a]	29.2	−167.3[a]	4.1
51297.7708	0.9490	...	...	...	...
51297.7840	0.9858	...	...	...	...
51662.7476	0.6888	32.2	−0.2	−311.4	−12.1
51662.7601	0.7237	22.3	−14.2	−304.6	11.8
51662.7739	0.7622	21.6	−15.6	−302.4	17.1
51662.7846	0.7921	8.6	−26.4	−295.5	14.8
51662.7969	0.8264	12.5	−17.2	−268.7	18.9
51662.8075	0.8560	−1.2	−24.0	−235.2	23.3
SW Lyn A					
51210.5716	0.6081	117.0	11.3	...	...
51210.5858	0.6301	121.3	3.8	−166.4[c]	−36.3
51210.6010	0.6537	120.6	−7.8	−180.2[c]	−29.4

Table 1—Continued

HJD–2,400,000	Phase	V_1	ΔV_1	V_2	ΔV_2
51210.6151	0.6756	126.9	−9.7	−176.5[c]	−10.0
51210.6316	0.7012	134.5	−9.2	−181.5[c]	−1.5
51210.6457	0.7231	132.0	−15.5	−176.7[c]	10.5
51210.6604	0.7459	143.2	−5.9	−177.3[c]	13.0
51210.6740	0.7670	128.8	−19.7	−183.3[c]	5.8
51210.6903	0.7924	137.9	−7.1	−167.5[c]	15.0
51210.7048	0.8149	139.1	−0.5	−172.8[c]	−0.7
51210.7200	0.8385	126.9	−4.7	−160.9[c]	−4.1
51210.7341	0.8604	132.2	10.0	−143.4[c]	−4.5
51210.7501	0.8852	131.0	21.5	−181.1[b]	···
51210.7655	0.9091	124.2	28.7	−167.5[b]	···
51254.5621	0.9093	108.8	13.4	−171.2[b]	···
51254.5747	0.9289	114.3	31.4	···	···
51570.5417	0.5106	···	···	···	···
51570.5505	0.5242	···	···	···	···
51570.5654	0.5474	···	···	···	···
51570.5780	0.5669	···	···	···	···
51570.5888	0.5837	···	···	···	···
51570.6041	0.6074	113.6	8.2	−189.5[b]	···
51570.6156	0.6253	127.9	12.8	−153.4[c]	−28.0
51570.6289	0.6460	112.7	−12.4	−179.6[c]	−35.2
51570.6397	0.6627	138.9	6.9	−159.4[c]	−1.7
51570.6540	0.6849	137.8	−1.7	−177.8[c]	−5.8
51570.6650	0.7020	148.7	4.8	−161.3[c]	19.0
51570.6773	0.7211	150.9	3.7	−198.1[c]	−11.4
51570.6883	0.7382	140.5	−8.3	−188.2[c]	1.5
51570.7027	0.7605	128.5	−20.4	−179.5[c]	10.4
51570.7141	0.7782	140.1	−7.2	−210.6[c]	−23.7
51570.7270	0.7983	134.3	−9.5	−178.5[c]	1.7
51570.7431	0.8233	130.4	−6.6	−204.9[c]	−37.7
51570.7543	0.8407	140.4	9.7	−190.0[c]	−34.8
51582.5277	0.1205	−46.5	1.3	169.8[a]	−15.5
51582.5422	0.1430	−67.5	−8.6	209.6[a]	3.0
51582.5592	0.1694	−75.2	−5.5	239.5[a]	12.3
51582.5734	0.1914	−73.3	3.2	232.5[a]	−7.7
51582.5894	0.2163	−77.0	4.7	260.8[a]	10.6
51582.6035	0.2381	−71.3	12.7	239.6[a]	−14.9
51582.6206	0.2647	−69.9	13.9	233.6[a]	−20.6
51582.6349	0.2869	−75.2	6.0	252.6[a]	3.4
51582.6516	0.3128	−68.2	7.2	236.3[a]	−1.7
51582.6659	0.3350	−72.7	−4.6	238.0[a]	13.9
51582.6828	0.3613	−61.8	−4.8	209.5[a]	6.6

Table 1—Continued

HJD–2,400,000	Phase	V_1	ΔV_1	V_2	ΔV_2
51582.6969	0.3832	−54.7	−8.9	189.4[a]	7.8
51582.7140	0.4097	−45.7	−15.4	169.5[a]	17.4
51582.7280	0.4315	−25.2	−8.9	···	···
51582.7439	0.4561	···	···	···	···
51582.7587	0.4791	···	···	···	···
51582.7759	0.5058	···	···	···	···
51582.7902	0.5280	···	···	···	···
51582.8061	0.5527	···	···	···	···
51582.8204	0.5749	···	···	···	···
51582.8371	0.6008	118.1	16.6	···	···
51582.8513	0.6229	132.6	18.8	−169.6[c]	−46.6
51582.8680	0.6488	136.6	10.3	−193.2[c]	−46.4
51582.8828	0.6718	138.7	3.4	−205.5[c]	−41.5
51582.9001	0.6987	144.9	1.8	−191.0[c]	−12.1
51582.9145	0.7210	140.8	−6.4	−178.7[c]	8.0
51589.6018	0.1040	−58.8	−20.3	191.1[a]	23.3
51589.6160	0.1260	−59.6	−8.9	206.3[a]	15.4
51589.6319	0.1507	−74.6	−12.3	230.3[a]	17.1
51589.6460	0.1726	−77.7	−6.9	230.2[a]	0.9
51589.6634	0.1996	−78.3	0.2	236.4[a]	−7.7
51589.6786	0.2232	−76.6	6.1	236.3[a]	−15.7
51589.6944	0.2477	−79.6	4.7	246.6[a]	−8.5
51589.7078	0.2685	−79.3	4.2	208.0[a]	−45.6
51589.7248	0.2949	−74.7	5.0	226.3[a]	−20.0
51589.7389	0.3168	−76.2	−2.0	227.0[a]	−8.8
51589.7549	0.3417	−62.6	2.9	216.2[a]	−3.0
V2377 Oph					
51675.7847	0.2866	35.1	−0.4	−185.7	−4.5
51675.7933	0.3068	28.6	−4.6	−179.3	−3.9
51675.8020	0.3273	26.7	−3.2	−170.6	−3.6
51675.8121	0.3510	23.1	−1.8	−152.3	2.0
51675.8207	0.3712	25.8	6.0	−136.7	4.6
51675.8293	0.3915	13.7	−0.2	−122.6	3.8
51675.8413	0.4197	−2.5	−7.2	−100.2	2.8
51675.8484	0.4364	···	···	···	···
51714.5841	0.4933	···	···	···	···
51714.5947	0.5182	···	···	···	···
51714.6072	0.5476	···	···	···	···
51714.6179	0.5727	···	···	···	···
51714.6312	0.6040	−63.0	1.1	69.9	−1.4
51714.6418	0.6289	−74.1	−2.7	83.2	−6.6
51714.6536	0.6566	−78.9	−0.6	106.0	−1.2

Table 1—Continued

HJD–2,400,000	Phase	V_1	ΔV_1	V_2	ΔV_2
51714.6644	0.6820	−78.2	4.9	123.9	4.4
51714.6823	0.7241	−87.1	0.8	131.7	−0.0
51714.6932	0.7497	−87.4	1.4	134.3	0.4
51714.7068	0.7817	−87.1	0.4	129.2	−1.5
51714.7179	0.8078	−88.6	−3.9	121.0	−2.4
51714.7326	0.8424	−80.8	−2.3	109.1	1.4
51714.7429	0.8666	−72.3	0.3	97.0	4.1
51764.5839	0.0290	...	...	...	...
51764.5925	0.0492	...	...	...	...
51764.6023	0.0722	...	...	...	...
51764.6108	0.0922	...	...	...	...
51764.6222	0.1190	19.9	2.9	−132.7	1.6
51764.6314	0.1406	28.3	5.4	−144.7	4.5
51764.6414	0.1641	29.1	0.8	−162.4	0.3
51764.6500	0.1843	29.1	−2.8	−175.2	−3.2
51764.6578	0.2027	34.4	−0.0	−179.0	−0.6
51764.6649	0.2194	33.7	−2.3	−183.4	−0.9
51764.6732	0.2389	38.9	1.8	−191.0	−6.0
51764.6822	0.2600	35.9	−1.2	−182.1	3.0
51764.6909	0.2805	32.6	−3.5	−182.4	0.1
51764.7018	0.3061	34.6	1.3	−175.7	−0.1
51764.7083	0.3214	34.6	3.6	−167.5	2.1
51764.7144	0.3357	33.7	5.4	−161.5	1.3
Anon Psc = GSC 00008–00324 (5184 Å)					
51782.6456	0.5781	30.2	−3.9	...	...
51782.6606	0.6267	64.8	−1.4	−161.4	0.5
51782.6785	0.6847	91.2	−1.6	−213.5	−13.6
51782.6946	0.7369	103.3	−0.0	−224.1	−9.3
51782.7098	0.7862	102.8	2.4	−203.5	7.1
51782.7264	0.8400	84.1	0.8	−191.7	−5.4
51782.7424	0.8918	58.5	3.6	−141.3	4.5
51782.7585	0.9440	...	...	...	...
51782.7739	0.9939	...	...	...	...
51782.7909	0.0490	...	...	...	...
51782.8068	0.1005	−102.7	2.9	77.7	−5.2
51782.8260	0.1628	−141.3	−1.1	108.7	−23.5
51782.8439	0.2208	−161.6	−4.3	...	...
51782.8597	0.2720	−156.7	1.5	...	...
51782.8753	0.3225	−148.7	−2.6	...	...
51782.8906	0.3721	−126.1	−3.5	...	...
51785.6288	0.2465	...	...	...	...
51785.6413	0.2871	...	...	...	...

Table 1—Continued

HJD–2,400,000	Phase	V_1	ΔV_1	V_2	ΔV_2
51793.6479	0.2362	−157.4	1.6	143.8	−15.2
51793.6588	0.2715	−154.4	3.9	155.1	−2.9
51793.6721	0.3146	−145.8	3.0	138.4	−6.0
51793.6840	0.3532	−130.4	2.4	124.7	3.1
51793.6960	0.3921	−101.7	8.8	···	···
51793.7073	0.4287	−71.3	13.6	···	···
51793.7200	0.4698	−48.6	4.1	···	···
51793.7307	0.5045	−26.0	−1.9	···	···
51793.7437	0.5467	1.2	−9.0	···	···
51793.7544	0.5813	39.3	2.8	···	···
51793.7675	0.6238	65.9	1.4	−156.1	3.4
51793.7787	0.6601	86.1	2.8	−177.0	9.3
51793.7927	0.7055	99.3	0.7	−207.3	0.8
51793.8040	0.7421	106.9	3.3	−222.6	−7.4
51793.8160	0.7810	100.5	−0.8	−225.9	−14.0
51793.8268	0.8160	96.8	4.2	−206.4	−6.9
51793.8388	0.8549	79.7	3.5	−181.5	−5.3
51793.8483	0.8857	71.3	12.5	−140.7	10.6
51793.8663	0.9440	···	···	···	···
51793.8765	0.9771	···	···	···	···
51793.8895	0.0192	···	···	···	···
51814.5450	0.9630	···	···	···	···
51814.5567	0.0009	···	···	···	···
51814.5708	0.0466	···	···	···	···
51814.5816	0.0816	−92.4	0.0	···	···
51814.5943	0.1227	−121.3	−1.7	117.3	14.5
51814.6052	0.1581	−138.8	−0.7	121.6	−7.6
51814.6191	0.2031	−153.4	0.4	132.8	−18.8
51814.6302	0.2391	−156.6	2.6	145.3	−13.9
51814.6428	0.2799	−151.4	5.8	153.1	−3.3
51814.6537	0.3152	−144.2	4.4	146.1	2.0
51814.6663	0.3561	−123.7	7.6	123.5	4.0
51814.6771	0.3911	−105.9	5.2	109.4	18.7
51814.6889	0.4293	−79.6	4.8	···	···
51814.6998	0.4647	−47.4	9.5	···	···
51814.7144	0.5120	−18.3	−0.3	···	···
51814.7252	0.5470	11.3	0.9	···	···
51814.7397	0.5940	46.7	1.3	−142.6	−10.3
51814.7505	0.6290	68.4	0.9	−162.0	1.8
51814.7642	0.6734	93.3	4.5	−176.6	17.5
51814.7751	0.7087	99.3	−0.0	−221.3	−12.1
51814.7869	0.7469	103.9	0.2	−227.4	−12.0

Table 1—Continued

HJD–2,400,000	Phase	V_1	ΔV_1	V_2	ΔV_2
51814.7977	0.7819	103.1	2.0	−210.9	0.8
51814.8086	0.8173	94.8	2.6	−202.1	−3.2
51814.8204	0.8555	79.4	3.5	−170.3	5.4
51814.8311	0.8902	59.3	3.4	−163.0	−15.8
51814.8442	0.9327	28.4	2.2	···	···
51814.8549	0.9673	···	···	···	···
51814.8669	0.0062	···	···	···	···
51814.8776	0.0409	···	···	···	···
Anon Psc = GSC 00008–00324 (5303 Å)					
51807.5787	0.3854	−107.5	7.2	103.9	8.1
51807.5893	0.4198	−84.1	7.4	102.1[a]	39.4
51807.6011	0.4580	−50.3	11.9	···	···
51807.6118	0.4927	−30.5	3.4	···	···
51807.6251	0.5358	−3.7	−5.2	···	···
51807.6359	0.5708	30.1	1.3	···	···
51807.6482	0.6107	58.4	2.0	−162.8	−14.8
51807.6588	0.6450	80.6	4.5	−170.1	6.0
51807.6708	0.6839	97.9	5.3	−188.5	11.0
51807.6815	0.7186	101.0	−0.2	−236.0	−24.2
51807.6947	0.7614	103.9	0.5	−232.1	−17.1
51807.7055	0.7964	102.6	4.4	−207.6	−0.1
51807.7180	0.8369	87.7	3.1	−189.3	−1.1
51807.7293	0.8735	69.9	3.8	−149.5	12.2
51807.7414	0.9127	44.3	3.6	−138.8	−13.1
51807.7521	0.9474	···	···	···	···
51807.7684	0.0002	···	···	···	···
51807.7791	0.0349	···	···	···	···
51807.7911	0.0738	···	···	···	···
51807.8017	0.1082	−114.1	−3.5	98.2	8.2
51807.8135	0.1464	−134.5	−1.9	126.8	5.5
51807.8241	0.1807	−149.0	−1.8	127.6	−14.6
51807.8374	0.2239	−156.6	1.1	163.4	6.2
51807.8480	0.2582	−158.1	1.2	146.7	−12.7
51807.8598	0.2965	−152.6	1.3	130.8	−20.9
51807.8707	0.3318	−138.8	3.7	140.1	4.6
51807.8824	0.3697	−117.3	6.7	95.2	−13.9
HT Vir B					
50610.6468	0.3870	−131.9	1.9	116.5	4.0
50630.5993	0.3298	−169.3	2.6	153.4	−6.1
50631.6693	0.9545	···	···	···	···
50651.6170	0.8855	113.5	25.2	−150.9	9.9
50858.9399	0.4412	−85.6[b]	···	73.7[b]	···

Table 1—Continued

HJD–2,400,000	Phase	V_1	ΔV_1	V_2	ΔV_2
50885.7348	0.1681	−184.9	−14.1	153.2	−5.0
50885.7423	0.1865	−181.0	−1.5	165.2	−3.6
50885.7496	0.2044	−187.2	−1.3	178.6	1.9
50896.6799	0.0161	...	...	...	...
50896.6882	0.0364	...	...	...	...
50896.6966	0.0570	...	...	...	...
50896.7067	0.0818	−123.9[b]	...	84.2[b]	...
50896.7146	0.1012	−153.5	−29.6	101.7	1.3
50896.7225	0.1205	−147.1	−7.3	127.2	7.3
50896.7315	0.1426	−162.3	−6.6	147.0	7.5
50896.7388	0.1605	−173.5	−6.8	156.8	3.7
50896.7460	0.1782	−184.2	−8.4	164.4	0.1
50896.7550	0.2003	−189.1	−4.5	172.3	−2.8
50896.7628	0.2194	−196.9	−7.3	167.0	−14.3
50896.7703	0.2378	−198.7	−6.4	184.0	−0.6
50896.7801	0.2618	−193.7	−1.4	180.1	−4.5
50896.7873	0.2795	−188.6	1.3	182.1	0.5
50896.7948	0.2979	−183.0	2.2	176.8	1.0
50896.8031	0.3183	−169.0	8.4	171.4	5.1
50896.8103	0.3359	−159.6	9.1	167.3	11.8
50922.6347	0.6823	111.6	−19.3	−218.3	−5.0
50922.6401	0.6955	127.1	−9.1	−221.6	−1.8
50922.6452	0.7080	134.2	−6.0	−221.1	3.6
50922.6507	0.7215	143.0	−0.3	−223.4	5.2
50922.6581	0.7396	145.1	−0.6	−225.5	6.0
50922.6647	0.7558	147.4	1.5	−231.2	0.6
50922.6724	0.7747	146.9	2.9	−202.9	26.5
50922.6807	0.7951	132.9	−6.4	−211.6	12.0
50922.6879	0.8127	135.3	2.3	−179.8	36.1
50922.6951	0.8304	114.8	−10.1	−204.9	1.0
50922.7023	0.8481	118.3	3.4	−185.6	8.0
50939.6174	0.3402	−152.0	14.3	163.5	10.9
50939.6232	0.3544	−148.3	9.3	157.1	15.2
50940.6072	0.7682	146.7	1.8	−219.6	11.0
50940.6148	0.7868	137.6	−3.9	−221.8	4.6
50940.7571	0.1359	−157.1	−6.1	132.4	−1.4
50941.6350	0.2893	−183.9	3.7	188.3	9.5
50948.6070	0.3914	−129.4	0.8	123.1	14.9
50949.5916	0.8066	136.3	0.9	−217.7	1.2
50951.6630	0.8876	109.9	23.4	−152.7	6.0
50960.6832	0.0139	...	...	...	...
50960.6903	0.0313	...	...	...	...

Table 1—Continued

HJD–2,400,000	Phase	V_1	ΔV_1	V_2	ΔV_2
50961.6897	0.4828	···	···	···	···
50961.6969	0.5004	···	···	···	···
50961.7041	0.5181	···	···	···	···
50961.7128	0.5394	···	···	···	···
50961.7200	0.5571	···	···	···	···
50961.7272	0.5748	78.0[b]	···	−126.7[b]	···
50961.7359	0.5961	94.0	21.2	−150.9	−9.1
50961.7431	0.6138	86.8	−0.9	−163.7	−3.6
50961.7504	0.6317	107.2	5.9	−181.2	−4.3
50961.7586	0.6518	121.0	6.2	−188.4	5.1
50961.7658	0.6694	112.5	−12.3	−211.5	−5.7
50965.5931	0.0577	···	···	···	···
51009.6010	0.0075	···	···	···	···
51232.7359	0.3495	−169.0	−8.2	152.4	6.6
51232.7433	0.3676	−156.5	−7.9	140.4	9.6
51232.7506	0.3855	−144.8	−9.8	133.3	19.3
51232.7609	0.4108	−127.1	−13.7	104.3	16.8
51232.7681	0.4284	−108.2	−11.2	102.8[b]	···
51232.7752	0.4459	−110.6[b]	···	79.0[b]	···
51232.7985	0.5030	···	···	···	···
51232.8064	0.5224	···	···	···	···
51232.8146	0.5425	···	···	···	···
51232.8247	0.5673	76.1[b]	···	−126.4[b]	···
51232.8339	0.5898	76.6	9.4	−142.9	−7.9
51232.8411	0.6075	90.4	7.9	−161.0	−7.2
51232.8506	0.6308	91.9	−8.8	−181.7	−5.6
51232.8583	0.6497	113.5	0.0	−199.8	−7.9
51232.8669	0.6708	124.7	−0.8	−212.6	−6.0
51232.8771	0.6958	132.3	−4.0	−220.4	−0.4
51232.8848	0.7147	134.6	−7.3	−226.4	0.4
51232.8927	0.7341	130.5	−14.7	−230.0	0.9
51232.9037	0.7611	136.9	−8.7	−225.1	6.3
51232.9115	0.7802	131.4	−11.6	−228.8	−0.6
51232.9193	0.7993	130.4	−7.5	−217.1	4.9
51232.9281	0.8209	123.2	−6.3	−213.4	−1.8
51232.9353	0.8386	118.7	−1.7	−200.0	0.4
51232.9426	0.8565	111.5	2.0	−187.1	−0.1
51232.9503	0.8754	98.1	2.0	−175.3	−4.8
51254.8208	0.5229	···	···	···	···
51261.8138	0.6765	112.9	−15.4	−216.3	−6.2
51267.6956	0.1044	−129.5	−2.8	107.7	3.9
51267.7062	0.1304	−146.8	0.3	128.1	−0.9

Table 1—Continued

HJD–2,400,000	Phase	V_1	ΔV_1	V_2	ΔV_2
51267.7183	0.1600	−174.2	−7.8	148.4	−4.3
51267.7290	0.1863	−179.7	−0.3	164.3	−4.4
51267.7430	0.2206	−185.8	4.1	178.8	−2.8
51267.7542	0.2481	−191.7	1.1	183.5	−1.7
51267.7664	0.2780	−193.6	−3.5	181.3	−0.6
51267.7773	0.3048	−184.2	−1.4	176.3	3.4
51267.7913	0.3391	−172.8	−5.9	156.6	3.3
51267.8026	0.3668	−149.2	−0.1	142.1	10.6
51267.8148	0.3968	−132.5	−6.8	120.1	17.5
51267.8493	0.4814	···	···	···	···
51267.8603	0.5084	···	···	···	···
51267.8750	0.5444	···	···	···	···
51267.8866	0.5729	72.5[b]	···	−132.7[b]	···
51267.8983	0.6016	74.9	−2.6	−161.3	−13.7
51267.9090	0.6278	98.4	−0.1	−176.3	−2.9
51267.9218	0.6592	108.8	−10.4	−199.5	−0.6
51297.7248	0.7649	139.9	−5.4	−226.7	4.3
51513.9792	0.2293	−195.7	−4.4	175.8	−7.6
51524.8606	0.9209	90.1[b]	···	−146.5[b]	···
51524.8689	0.9413	83.8[b]	···	−102.6[b]	···
51524.8770	0.9612	···	···	···	···

[a]These data have been given half weight in the orbital solution.

[b]These data have not been used in the orbital solution.

[c]The data for the secondary component of SW Lyn between phases 0.5 – 1.0 have been given quarter weight in the orbital solution.

Note. — Velocities are expressed in km s^{-1}. Observations leading to entirely unseparable broadening- and correlation-function peaks are marked by the “no-data” symbol (···); these observations may be eventually used in more extensive modeling of broadening functions.

Table 2. Spectroscopic orbital elements of the fourth ten of close binary systems

Name	Type Sp. type	Other names	V_0	K_1 K_2	ϵ_1 ϵ_2	T_0 – 2,400,000 (O–C), [E]	P (days) $(M_1+M_2)\sin^3 i$	q
44 Boo B[a]	EW/W (K2 V)	HD 133640B HIP 73695	−17.89 (0.40)	231.31 (0.65) 112.70 (0.46)	5.50 3.29	50,944.6878(2) +0.0002 [8]	0.267818 1.132 (11)	0.487 (6)
FI Boo[b]	EW/W G3 V	HD 234224 HIP 75203	−30.55 (0.72)	148.65 (1.10) 55.27 (0.90)	5.17 4.52	51,718.3951 (7) +0.0926 [8,252]	0.389998 0.343 (10)	0.372 (21)
V2150 Cyg	EW/A A6 V	HD 202924 HIP 105162	−12.82 (0.45)	125.43 (0.55) 156.40 (0.66)	3.18 5.69	51,386.3434 (7) +0.0195 [4,876]	0.591856 1.376 (18)	0.802 (6)
V899 Her B[a]	EW/A F5 comp.	HD 149684 HIP 81191	−16.84 (1.30)	135.97 (2.04) 240.37 (2.12)	14.9 14.5	51,533.8405 (11) −0.0046 [7,203]	0.421173 2.331 (77)	0.566 (18)
EX Leo	EW/A F6 V	BD 17°2269 HIP 52580	−11.05 (1.10)	51.28 (1.07) 257.98 (1.85)	3.23 20.1	51,615.6025 (13) −0.0110 [7,625]	0.408604 1.255 (36)	0.199 (36)
VZ Lib A[a]	EW/A G0 comp.	 HIP 76050	−31.11 (2.30)	68.54 (3.84) 289.25 (4.55)	18.5 27.7	51,091.4297 (15) −0.0814 [17,593]	0.358263 1.704 (120)	0.237 (68)
SW Lyn A[a,c]	EB (F2 V)	HD 67008 HIP 39771	+32.39 (1.35)	116.73 (1.65) 222.75 (3.20)	11.2 19.1	51,400.1795 (25) −0.0062 [801]	0.644066 2.617 (112)	0.524 (28)
V2377 Oph	EW/W G0/1 V	HD 159356 HIP 85944	−25.79 (0.38)	159.64 (0.70) 62.99 (0.62)	3.18 3.16	51,720.3294 (5) +0.0128 [7,570]	0.425401 0.487 (9)	0.395 (12)
Anon Psc	EB? EA? (K4/5 V)	GSC 8–324[d]	−27.85 (0.73)	131.62 (0.55) 187.55 (1.80)	4.44 11.6	51,794.1921 (4) −0.0188 [1,110]	0.308550 1.042 (23)	0.702 (14)
HT Vir B[a]	EW/A F8 V comp.	HD 119931 HIP 67186	−23.38 (0.68)	169.39 (1.00) 208.54 (1.00)	9.32 9.45	51,068.7101 (6) +0.0382 [17,230]	0.407670 2.285 (38)	0.812 (8)

[a]Spectroscopically triple system.

[b]FI Boo: The period is twice the value given in the Hipparcos catalogue where the time of maximum light is given as the initial epoch. The large O–C reflects this difference.

[c]The solution for SW Lyn A is based on both observational seasons. See the text for discussion concerning the possible influence of the motion around the common center of mass in the triple system.

[d]The Guide Star Catalogue number is written in an abbreviated form in the table. The correct number is: GSC 00008–00324.

Note. — The spectral types given in column two are new except those in parantheses which are either taken from the literature or estimated from color indices. The convention of naming the binary components is that the subscript 1 designates the component which is eclipsed at the deeper minimum and is therefore the hotter one. The standard errors of the circular solutions in the table are expressed in units of last decimal places quoted; they are given in parantheses after each value. For example, the last table entry for the mass ratio q, 0.812 (8), should be interpretted as $q = 0.812 \pm 0.008$; the mass ratio is defined to be always $q \leq 1$. The center-of-mass velocities (V_0), the velocity amplitudes (K_i) and the standard unit-weight errors of the solutions (ϵ) are expressed in km s^{-1}. The spectroscopically determined moments of primary minima are given by T_0; the corresponding (O–C) deviations (in days) have been calculated from the most recent available ephemerides, as given in the text, using the assumed periods and the number of epochs given by [E]. The values of $(M_1 + M_2)\sin^3 i$ are in the solar mass units.

Table 3. Observations of the spectroscopic companions of close binary systems

HJD–2,400,000	V	Weight
44 Boo A		
50939.6449	−35.3	1.0
50948.6671	−34.2	1.0
50949.6755	−35.3	1.0
V899 Her A		
51402.5597	5.6	1.0
51402.5671	5.5	1.0
51402.5745	3.4	1.0
51402.5827	5.1	1.0
51402.5908	3.8	1.0
51402.5987	4.0	1.0
51402.6073	4.1	1.0
51402.6147	3.0	1.0
51456.5091	−10.8	1.0
51456.5197	−9.8	1.0
51456.5328	−9.7	1.0
51456.5437	−8.6	1.0
51456.5518	−7.8	1.0
51466.4905	−12.7	1.0
51466.4977	−12.6	1.0
51466.5049	−12.1	1.0
51466.5130	−12.0	1.0
51466.5201	−11.5	1.0
51466.5273	−11.9	1.0
51466.5354	−11.1	1.0
51466.5464	−12.7	1.0
51466.5540	−12.1	1.0
51466.5621	−13.2	1.0
51634.7840	−9.5	1.0
51634.7946	−9.3	1.0
51634.8066	−9.6	1.0
51634.8173	−9.3	1.0
51634.8294	−10.5	1.0
51634.8401	−10.9	1.0
51634.8639	−10.4	1.0
51634.8746	−10.1	1.0
51634.8871	−10.2	1.0
51635.8276	−10.9	1.0
51635.8386	−11.1	1.0
51635.8494	−10.3	1.0
51635.8709	−11.6	1.0
51635.8819	−10.5	1.0

Table 3—Continued

HJD–2,400,000	V	Weight
51635.8937	−10.4	1.0
51635.9051	−10.4	1.0
51647.7633	−8.9	1.0
51647.7712	−10.3	1.0
51647.7786	−9.8	1.0
51647.7859	−10.5	1.0
51647.7972	−8.9	1.0
51647.8045	−8.9	1.0
51647.8119	−10.0	1.0
51647.8225	−10.9	1.0
51647.8298	−10.0	1.0
51647.8375	−10.4	1.0
51647.8487	−9.5	1.0
51647.8560	−10.5	1.0
51647.8632	−9.3	1.0
51647.8737	−10.6	1.0
51647.8810	−9.4	1.0
51647.8882	−9.5	1.0
51663.5826	−7.2	1.0
51663.5932	−7.0	1.0
51663.6068	−6.5	1.0
51663.6182	−7.1	1.0
51663.6307	−7.1	1.0
51663.6414	−7.2	1.0
51663.6535	−6.4	1.0
51663.6642	−5.6	1.0
51663.6774	−7.1	1.0
51663.6884	−8.0	1.0
VZ Lib B		
50520.8497	−20.1	1.0
50520.8605	−22.6	1.0
50520.8727	−22.2	1.0
50520.8835	−17.9	1.0
50520.8970	−19.3	1.0
50520.9095	−20.4	1.0
50520.9229	−22.1	1.0
50520.9338	−20.7	1.0
50539.9024	−19.5	1.0
50540.7525	−8.9	1.0
50540.7632	−14.8	1.0
50540.7754	−16.6	1.0
50540.7871	−15.9	1.0

Table 3—Continued

HJD–2,400,000	V	Weight
50540.8005	−13.1	1.0
50540.8113	−15.6	1.0
50540.8235	−22.2	1.0
50541.8017	−12.9	1.0
50541.8124	−14.9	1.0
50541.8246	−16.5	1.0
50596.6337	−10.1	1.0
50596.6445	−16.9	1.0
50596.6571	−11.9	1.0
50596.6678	−14.3	1.0
50596.6799	−11.9	1.0
50596.6905	−13.9	1.0
50930.7689	−29.6	1.0
50930.7796	−29.8	1.0
50930.7916	−28.5	1.0
50930.8029	−31.4	1.0
50930.8150	−26.2	1.0
51254.8413	−47.3	1.0
51254.8521	−48.2	1.0
51254.8667	−50.7	1.0
51254.8775	−45.9	1.0
51281.7208	−38.9	1.0
51281.7321	−40.5	1.0
51281.7443	−44.1	1.0
51281.7552	−33.3	1.0
51281.7690	−43.0	1.0
51281.7808	−41.1	1.0
51281.7935	−42.1	1.0
51281.8045	−46.1	1.0
51281.8177	−44.3	1.0
51281.8295	−41.8	1.0
51281.8424	−42.2	1.0
51281.8536	−44.1	1.0
51281.8667	−37.6	1.0
51281.8779	−38.3	1.0
51281.8906	−40.3	1.0
51281.9021	−43.9	1.0
51297.7375	−36.3	1.0
51297.7484	−39.6	1.0
51297.7602	−39.1	1.0
51297.7708	−42.8	1.0
51297.7840	−42.3	1.0

Table 3—Continued

HJD–2,400,000	V	Weight
51662.7476	−12.8	1.0
51662.7601	−22.5	1.0
51662.7739	−24.4	1.0
51662.7846	−18.3	1.0
51662.7969	−21.8	1.0
51662.8075	−16.4	1.0
SW Lyn B		
51210.5716	26.6	1.0
51210.5858	24.5	1.0
51210.6010	23.5	1.0
51210.6151	24.2	1.0
51210.6316	25.9	1.0
51210.6457	24.5	1.0
51210.6604	25.4	1.0
51210.6740	25.1	1.0
51210.6903	24.5	1.0
51210.7048	24.2	1.0
51210.7200	24.5	1.0
51210.7341	24.1	1.0
51210.7501	27.8	1.0
51210.7655	23.7	1.0
51254.5621	27.4	1.0
51254.5747	29.4	1.0
51570.5417	0.0	0.0
51570.5505	0.0	0.0
51570.5654	0.0	0.0
51570.5780	40.4	1.0
51570.5888	36.6	1.0
51570.6041	35.1	1.0
51570.6156	37.4	1.0
51570.6289	37.0	1.0
51570.6397	38.2	1.0
51570.6540	36.9	1.0
51570.6650	40.6	1.0
51570.6773	35.5	1.0
51570.6883	36.8	1.0
51570.7027	35.1	1.0
51570.7141	37.8	1.0
51570.7270	36.6	1.0
51570.7431	37.7	1.0
51570.7543	38.6	1.0
51582.5277	38.1	1.0

Table 3—Continued

HJD–2,400,000	V	Weight
51582.5422	37.6	1.0
51582.5592	36.9	1.0
51582.5734	35.8	1.0
51582.5894	34.7	1.0
51582.6035	35.5	1.0
51582.6206	38.0	1.0
51582.6349	35.1	1.0
51582.6516	36.1	1.0
51582.6659	36.2	1.0
51582.6828	36.8	1.0
51582.6969	36.9	1.0
51582.7140	39.4	1.0
51582.7280	40.0	1.0
51582.7439	41.9	1.0
51582.7587	0.0	0.0
51582.7759	0.0	0.0
51582.7902	0.0	0.0
51582.8061	0.0	0.0
51582.8204	35.8	1.0
51582.8371	38.5	1.0
51582.8513	37.6	1.0
51582.8680	39.4	1.0
51582.8828	37.9	1.0
51582.9001	40.4	1.0
51582.9145	38.5	1.0
51589.6018	33.2	1.0
51589.6160	34.1	1.0
51589.6319	33.9	1.0
51589.6460	33.1	1.0
51589.6634	33.7	1.0
51589.6786	34.2	1.0
51589.6944	34.1	1.0
51589.7078	33.5	1.0
51589.7248	35.0	1.0
51589.7389	33.2	1.0
51589.7549	33.9	1.0
HT Vir A		
50610.6468	−29.3	1.0
50630.5993	−25.0	1.0
50631.6693	−28.3	1.0
50651.6170	−16.1	1.0
50858.9399	−31.3	1.0

Table 3—Continued

HJD–2,400,000	V	Weight
50885.7348	−17.9	0.6
50885.7423	−18.3	0.6
50885.7496	−17.9	0.6
50896.6799	−32.2	0.2
50896.6882	−32.3	0.2
50896.6966	−33.2	0.2
50896.7067	−32.4	0.2
50896.7146	−32.9	0.2
50896.7225	−33.3	0.2
50896.7315	−33.0	0.2
50896.7388	−33.7	0.2
50896.7460	−35.0	0.2
50896.7550	−34.1	0.2
50896.7628	−34.6	0.2
50896.7703	−34.8	0.2
50896.7801	−32.7	0.2
50896.7873	−33.9	0.2
50896.7948	−34.3	0.2
50896.8031	−33.7	0.2
50896.8103	−33.7	0.2
50922.6347	−22.8	0.3
50922.6401	−22.5	0.3
50922.6452	−22.4	0.3
50922.6507	−23.4	0.3
50922.6581	−21.8	0.3
50922.6647	−22.3	0.3
50922.6724	−24.0	0.3
50922.6807	−19.7	0.3
50922.6879	−22.6	0.3
50922.6951	−23.8	0.3
50922.7023	−22.7	0.3
50939.6174	−15.0	0.7
50939.6232	−15.1	0.7
50940.6072	−16.0	0.6
50940.6148	−14.9	0.6
50940.7571	−17.5	0.6
50941.6350	−13.9	1.0
50948.6070	−14.2	1.0
50949.5916	−14.5	1.0
50951.6630	−20.1	1.0
50960.6832	−33.9	0.7
50960.6903	−34.0	0.7

Table 3—Continued

HJD–2,400,000	V	Weight
50961.6897	−32.7	0.3
50961.6969	−32.4	0.3
50961.7041	−33.3	0.3
50961.7128	−33.5	0.3
50961.7200	−32.9	0.3
50961.7272	−33.2	0.3
50961.7359	−32.3	0.3
50961.7431	−33.5	0.3
50961.7504	−33.8	0.3
50961.7586	−34.1	0.3
50961.7658	−34.6	0.3
50965.5931	−32.5	1.0
51009.6010	−14.8	1.0
51232.7359	−15.7	0.2
51232.7433	−14.6	0.2
51232.7506	−12.6	0.2
51232.7609	−14.9	0.2
51232.7681	−14.3	0.2
51232.7752	−14.8	0.2
51232.7985	−13.0	0.2
51232.8064	−15.2	0.2
51232.8146	−14.5	0.2
51232.8247	−15.9	0.2
51232.8339	−14.1	0.2
51232.8411	−15.6	0.2
51232.8506	−13.1	0.2
51232.8583	−14.2	0.2
51232.8669	−15.7	0.2
51232.8771	−16.9	0.2
51232.8848	−15.0	0.2
51232.8927	−14.1	0.2
51232.9037	−13.8	0.2
51232.9115	−15.1	0.2
51232.9193	−14.4	0.2
51232.9281	−15.7	0.2
51232.9353	−15.1	0.2
51232.9426	−15.2	0.2
51232.9503	−16.0	0.2
51254.8208	−34.2	1.0
51261.8138	−19.6	1.0
51267.6956	−13.2	0.2
51267.7062	−13.4	0.2

Table 3—Continued

HJD–2,400,000	V	Weight
51267.7183	−14.2	0.2
51267.7290	−15.1	0.2
51267.7430	−14.0	0.2
51267.7542	−15.3	0.2
51267.7664	−14.8	0.2
51267.7773	−15.4	0.2
51267.7913	−14.6	0.2
51267.8026	−15.2	0.2
51267.8148	−16.0	0.2
51267.8493	−15.5	0.2
51267.8603	−15.6	0.2
51267.8750	−15.6	0.2
51267.8866	−14.6	0.2
51267.8983	−15.9	0.2
51267.9090	−16.4	0.2
51267.9218	−16.4	0.2
51297.7248	−14.2	1.0
51513.9792	−32.1	1.0
51524.8606	−17.1	0.6
51524.8689	−15.6	0.6
51524.8770	−17.1	0.6
51564.8586	−17.7	1.0
51634.6281	−23.0	0.7
51634.6356	−23.4	0.7
51649.6919	−27.9	1.0
51662.8205	−18.7	1.0
51663.5555	−16.8	1.0
51664.5612	−19.6	1.0
51665.5567	−19.4	1.0
51668.5883	−25.5	1.0
51670.5660	−27.7	1.0
51671.5648	−26.8	1.0
51673.5817	−27.7	1.0
51675.5917	−31.8	1.0
51702.5886	−26.2	1.0
51704.6493	−31.0	1.0
51717.5910	−16.6	1.0

Note. — Velocities in the second column are expressed in km s^{-1}. Weights have been assigned on the basis of quality of the radial velocity determinations from broadening functions. A weight equal to zero means that we were not able to use this spectrum for radial velocity determination.

Table 4. Preliminary spectroscopic orbit for HT Vir A

Element	Unit	Value
Period	day	32.450 ± 0.012
V_0	km s^{-1}	-23.15 ± 0.17
K_1	km s^{-1}	10.10 ± 0.24
e		0.232 ± 0.028
ω	radian	4.204 ± 0.088
T_0	JD	$2,451,194.33 \pm 0.45$
σ	km s^{-1}	1.65